Production of particulate brown carbon during atmospheric aging of residential wood-burning emissions

Nivedita K. Kumar[1], Joel C. Corbin[1*], Emily A. Bruns[1], Dario Massabó[2], Jay G. Slowik[1], Luka Drinovec[3,4], Griša Močnik[3,4], Paolo Prati[2], Athanasia Vlachou[1], Urs Baltensperger[1], Martin Gysel[1], Imad El-Haddad[1] and André S. H. Prévôt[1]

[1]Laboratory of Atmospheric Chemistry, Paul Scherrer Institute, 5232 Villigen, Switzerland

[2]Department of Physics & INFN, University of Genoa, via Dodecaneso 33, 16146, Genova, Italy

[3]Aerosol d.o.o, Kamniška 41, 1000 Ljubljana, Slovenia

[4]Condensed Matter Physics, Jožef Stefan Institute, 1000 Ljubljana, Slovenia

*Now at National Research Council Canada, Ottawa, Canada

Correspondence to: I. El-Haddad (imad.el-haddad@psi.ch), A. S. H. Prévôt (andre.prevot@psi.ch)

ABSTRACT

We investigate the optical properties of light-absorbing organic carbon (brown carbon) from domestic wood combustion as a function of simulated atmospheric aging. At shorter wavelengths (370 – 470nm), light absorption by brown carbon from primary organic aerosol (POA) and secondary organic aerosol (SOA) formed during aging was around 10 % and 20 %, respectively, of the total aerosol absorption (brown carbon plus black carbon). The mass absorption cross-section (MAC) determined for black carbon (BC, 13.7 $m^2 g^{-1}$ (geometric standard deviation GSD = 1.1) at 370 nm) was consistent with that recommended by Bond et al. (2006). The corresponding MAC of POA (5.5 $m^2 g^{-1}$ (GSD =1.2)) was higher than that of SOA (2.4 $m^2 g^{-1}$ (GSD = 1.3)) at 370 nm. However, SOA presents a substantial mass fraction, with a measured average SOA/POA mass ratio after aging of ~5 and therefore contributes significantly to the overall light absorption, highlighting the importance of wood-combustion SOA as a source of

22   atmospheric brown carbon. The wavelength dependence of POA and SOA light absorption between 370 nm and 660

23   nm is well described with absorption Ångström exponents of 4.6 and 5.6, respectively. UV-visible absorbance

24   measurements of water and methanol-extracted OA were also performed showing that the majority of the light-

25   absorbing OA is water insoluble even after aging.

26

1. INTRODUCTION

28   Atmospheric aerosols contribute to radiative forcing either directly by absorbing and scattering light or indirectly by

29   acting as cloud-condensation and ice nuclei. While black carbon (BC) from combustion processes is the most

30   efficient light-absorbing aerosol component, organic aerosols (OA) may also absorb solar radiation (Alexander et

31   al., 2008; Chen and Bond, 2009; Kirchstetter et al., 2004). This light-absorbing OA, denoted as brown carbon

32   (BrC), absorbs most strongly at shorter UV-visible wavelengths (Andreae and Gelencsér, 2006; Hoffer et al., 2005).

33   Global chemical-transport model estimates indicate that the BrC contribution to the positive radiative forcing of

34   climate by anthropogenic aerosols may not be negligible (Feng et al., 2013; Jo et al., 2016; Lin et al., 2014; Wang et

35   al., 2014).

36   Unlike BC, whose light absorption properties are relatively constant across sources (Bond et al., 2013), BrC is

37   composed of a wide range of largely unknown compounds, which exhibit highly variable spectral dependence and

38   absorption efficiencies. For example, reported imaginary indices of refraction for different organic species, which

39   describe the absorption of these compounds, span two orders of magnitude (Lu et al., 2015). Because it is

40   impractical to experimentally separate BrC from non-absorbing OA, optical properties are typically determined for

41   the bulk OA of a given source. The large variability of BrC fraction in combustion aerosol may contribute to the

42   wide variation in reported properties of BrC containing OA.

43   Biomass burning OA, which contributes two-thirds of the global budget of directly-emitted primary OA (POA), is

44   expected to be a considerable source of BrC (Chakrabarty et al., 2010; Hecobian et al., 2010; Lack and Langridge,

45   2013; Liu et al., 2014). The variability in reported light absorption properties of biomass burning OA with fuel type

46   and burn conditions remains a major obstacle complicating its treatment in climate models (Lu et al., 2015; Saleh et

47 al., 2013). Residential biomass burning is typically characterized by a more efficient combustion, than open burning.

48 Residential wood burning represents a substantial contribution to anthropogenic combustion emissions (Bond et al.,

49 2013), especially in urban atmospheres, and is considered the largest source of OA in Europe during winter (Denier

50 Van Der Gon et al., 2015).

51 Upon photo-oxidation, biomass-burning emissions produce secondary organic aerosol (SOA) at concentrations

52 similar to or exceeding the primary organic aerosol (POA) (Bertrand et al., 2017; Bruns et al., 2015, 2016; Corbin et

53 al., 2015a; Grieshop et al., 2009). There is a growing body of evidence that light absorption by OA change with OH

54 exposure (aging) owing to the production of secondary BrC or to the transformation of primary BrC (Forrister et al.,

55 2015; Heringa et al., 2011; Lee et al., 2014; Zhao et al., 2015). However, these effects have not yet been

56 systematically investigated and must be quantified to assess the climate effects of primary and aged biomass burning

57 OA.

58 Here, we show that both POA and SOA from residential biomass burning emissions aged in controlled smog

59 chamber experiments contain BrC. Wavelength dependent, mass-normalized absorption cross-sections (MACs) of

60 POA and SOA are presented from online aerosol measurements as a function of aging for the first time.

61 Complementary measurements of filter-extract absorbance (conducted in different solvents) are used to obtain the

62 imaginary refractive index and to investigate the solubility of BrC in fresh and aged OA. While results presented

63 here are related to flaming residential wood combustion emissions and cannot therefore be generalized, the approach

64 used can be extrapolated for the characterization and quantification of the contribution of BrC in other primary and

65 aged emissions.

66

67 **2. METHODS**

68 **2.1 Smog chamber experiments**

69 Laboratory measurements were conducted in an 8 m^3 Teflon smog chamber (Bruns et al., 2015; Platt et al., 2013)

70 installed within a temperature-controlled housing. Conditions in the chamber were maintained to represent winter

71 time in Europe, i.e. relative humidity ranging between 50 – 90%, at 263 K (Bruns et al., 2015, 2016). Beech wood

72 was combusted in a residential wood stove. Primary emissions were sampled through heated lines at 413 K, diluted

73 by a factor of ~14 using an ejector diluter (DI-1000, Dekati Ltd.), then sampled into the chamber, which provided an

74 additional ten-fold dilution. The overall dilution was a factor of 100 to 200. As we aimed to sample only flaming-

75 phase emissions into the chamber, samples were taken when the modified combustion efficiency (ratio of CO_2 to the

76 sum of CO and CO_2) was > 0.90. Despite maintaining the same combustion conditions, the resulting organic fraction

77 to the total carbonaceous aerosols in the different samples was highly variable, indicating that these samples are

78 representative of a mixture of pre- ignition and flaming emissions (with varying contributions of each combustion

79 stage). Finally, the resulting NOx/NMOG ratios, which dramatically influence SOA formation through influencing

80 the fate of peroxy radicals, RO_2, were estimated to be between 0.035 – 0.35 ppm ppm C^{-1} (Bruns et al., 2016). These

81 conditions can be considered as high NO_X representative of urban/sub-urban conditions, where most of the RO_2

82 radicals react with NO, rather with RO_2/HO_2.

83 After injection of the primary emissions and stabilization of the concentrations, nitrous acid (HONO) was

84 continuously added, which dissociates upon irradiation (λ<400 nm) and forms the hydroxyl radical (OH). Then, 9-

85 times deuterated butanol sample (butanol- D9, 98%, Cambridge Isotope Laboratories) was subsequently injected

86 into the chamber. The decay of butanol-D9 was used to infer the time-resolved OH exposure of the sampled aerosol

87 (Barmet et al., 2012). The chamber was exposed to UV lights for ~3.5 hours.

88 Particles were collected onto filters (47 mm Tissue-quartz, Pall Corporation, 26 L min^{-1} for 30-32 min) for offline

89 optical measurements and the determination of elemental carbon (EC) mass. Three filters were collected during each

90 experiment, namely i) a primary aerosol filter sample ("primary"), ii) a slightly aged aerosol ("Aged1", OH

91 exposure ~ $1x10^7$ molecules cm^{-3} h), collected 30 minutes after the UV lights were switched on, and iii) an aged

92 aerosol ("Aged2", OH exposure ~ $4x10^7$ molecules cm^{-3} h), collected at the end of the experiment (see Fig. S1 for

93 the sampling periods). A charcoal denuder was installed upstream of the filter sampler to remove organic gases.

94 Filters were stored at 253K until analysis.

95 In addition to the characterization of the particle optical properties detailed in the next section, a set of online and

96 offline techniques were used for the characterization of the gaseous and particulate emissions before and after aging.

97 The non-refractory particle size-segregated chemical composition was measured with a high resolution (HR) time-

98 of-flight aerosol mass spectrometer (AMS) (DeCarlo et al., 2006). Uncertainties related to particle collection

99 efficiency in the AMS are considered negligible for the relatively-large particles sampled here, which in terms of

100 volume are within the size range transmitted efficiently by the AMS aerodynamic lens (Liu et al., 2007). The

101 collection efficiency of wood-combustion OA is expected to be unity (Corbin et al., 2015b). Details related to the

102 AMS data analysis and calibration can be found elsewhere (Bruns et al., 2015, 2016). A scanning mobility particle

103 sizer was used to measure the size distribution of the evolving aerosol. Organic gases were monitored by a proton

104 transfer reaction time-of-flight mass spectrometer (PTR-MS, $[H_3O^+]$ reagent ion, Ionicon Analytik GmbH) (Bruns et

105 al., 2017), following the same procedure as in Klein et al. (2016). Additionally, elemental carbon (EC) mass

106 concentration was measured offline using a sunset thermo-optical analyzer, following the EUSAAR2 protocol

107 (Cavalli et al., 2010).

108 **2.2 Optical measurements**

109 **Aethalometer.** A dual-spot aethalometer (Magee Scientific aethalometer AE33, Aerosol d.o.o.) was used for real-

110 time aerosol light attenuation measurements at seven wavelengths (λ = 370, 470, 520, 590, 660, 880 and 950 nm)

111 (Drinovec et al., 2015). The instrument measures the attenuation coefficient (b_{ATN}) of a light beam transmitted

112 through a filter tape loaded with aerosol samples. The use of the sampling flow (here, 2 L min⁻¹), integration time for

113 the measurement (here, 1 minute), and automated dual-spot loading compensation to obtain b_{ATN} has been described

114 by Drinovec et al. (2015).

115 The loading compensated b_{ATN} was used to infer the aerosol absorption coefficient, b_{abs}, using a constant wavelength

116 independent correction factor C, which accounts for multiple scattering within the filter matrix (Weingartner et al.,

117 2003):

118 $b_{abs}(\lambda) = b_{ATN}(\lambda)/C$ (1)

119 As discussed in detail by Corbin et al. (2018), the wavelength-dependence of C can be expected to be negligible.

120 The loading compensated b_{ATN} at 880 nm from the AE33 is further used to infer the equivalent-BC mass

121 concentration, M_{eBC}:

122 $M_{eBC} = \frac{b_{ATN}(880\ nm)}{\sigma_{ATN}(880\ nm)}$ (2)

123 where σ_{ATN} is the mass attenuation cross-section of BC deposited on the filter of the AE33. M_{eBC} inferred from Eq.

124 (2) only equals the true BC mass concentration, M_{BC}, if the applied σ_{ATN} is identical to the true attenuation cross-

125   section of BC, $\sigma_{\text{ATN,BC}}$, and if light attenuation at 880 nm is exclusively due to BC. $\sigma_{\text{ATN,BC}}(880\ nm)$ can be

126   inferred from the true MAC of BC, MAC_{BC}, and the true C value:

127    $\sigma_{\text{ATN,BC}}(880\ nm) = \text{MAC}_{\text{BC}}(880\ nm) * C$ (3)

128   with MAC_{BC} being defined as:

129    $\text{MAC}_{\text{BC}}(\lambda) = \dfrac{b_{\text{abs,BC}}(\lambda)}{M_{\text{BC}}}$ (4)

130   where $b_{\text{abs,BC}}$ is the absorption coefficient due to BC.

131   The manufacturer default values are 1.57 for C (TFE-coated glass fiber filters) and 12.2 m^2g^{-1} for σ_{ATN} at 880 nm,

132   which corresponds to a $\text{MAC}_{\text{BC}}(880\ \text{nm})$ of 7.77 m^2g^{-1} (Gundel et al., 1984 , Drinovec et al., 2015). However, these

133   three parameters depend on aerosol properties. Here, we have determined the C value by applying Eq. (1) to b_{ATN}

134   measured by the aethalometer and the absorption coefficient, $b_{\text{abs}_{\text{MWAA}}}$, measured by a multi-wavelength

135   absorbance analyser, MWAA (Massabò et al., 2015; Massabò et al., 2013). The $\text{MAC}_{\text{BC}}(880\ \text{nm})$ was determined

136   using Eq. (4) to compare $b_{\text{abs}_{\text{MWAA}}}$ from the MWAA measurements with EC mass from the Sunset thermo-optical

137   analyzer (see Fig. 1A&B and Section 4.1 for detailed discussion). Following this procedure, the MWAA and Sunset

138   analyser will be defined as reference methods for absorption coefficient and EC mass concentration, respectively.

139   Note that data from these reference methods were only available with low time resolution and for a subset of all

140   samples. Thus, the aethalometer anchored against these reference methods, was used to obtain the wavelength

141   dependent absorption coefficients and the eBC mass concentrations with high time resolution using Eq. (1) and (2),

142   respectively. Processing the loading compensated AE33 attenuation coefficients with C value and MAC_{BC},

143   determined with independent MWAA and Sunset analyser measurements, ensures that the inferred $b_{\text{abs}}(\lambda)$ (Eq. (1))

144   and M_{eBC} (Eq. (2)) have minimal bias compared to respective true values.

145   **MWAA measurements.** The MWAA (Massabò et al., 2015; Massabò et al., 2013) was used as reference method

146   for the aerosol absorption coefficient. It measures the absorption coefficient $b_{\text{abs}_{\text{MWAA}}}(\lambda)$ of particles deposited on

147   on standard filter samples. It is composed of five laser diodes, with λ = 375, 407, 532, 635 and 850 nm, acting as

148   light sources and placed above the filter, an automated sample-changer, and three low-noise UV-enhanced

149   photodiodes. The first photodiode is placed behind the filter for transmittance measurements (0° relative to the

150 incident light, 1.5 cm from the sample), while the other two photodiodes are positioned at 125º and 165º (11 cm

151 from the sample) to collect the back scattered light. These transmittance and reflectance measurements are used

152 together with a radiative transfer model (Hänel et al., 1987) , which takes into account multiple scattering within the

153 particle/filter layer, to retrieve both the total optical thickness and the particle-filter-layer single scattering albedo,

154 providing the absorption coefficient $b_{abs_{MWAA}}(\lambda)$ values. These calculations largely follow the approach

155 implemented in the multi-angle absorption photometer (MAAP, Petzold and Schönlinner, 2004).

156 **UV-visible absorbance measurements of extracted aerosols.** Filter samples were extracted for UV-visible

157 absorbance measurements in 10 mL ultrapure water or methanol in an ultrasonic bath for 20 min at 30 °C. Samples

158 were subsequently briefly vortexed (1 min) and filtered with 0.45 µm nylon membrane syringe filters following the

159 procedure described in Daellenbach et al. (2016). Absorption spectra were measured from 280 to 500 nm using a

160 UV-visible spectrophotometer (Ocean Optics) coupled to a 50-cm long-path detection cell (Krapf et al., 2016). Light

161 attenuation by the OA in solution, $ATN_{OA\text{-}sol}$, at a given wavelength was recorded as the logarithm of the ratio of

162 signal intensities of the reference (solvent) (I_0) and the sample (I), both corrected for background signals with the

163 light source off. From $ATN_{OA\text{-}sol}$, the absorption coefficient of OA in solution, $b_{abs,OA-sol}(\lambda)$, can be quantified as:

164 $$b_{abs,OA-sol}(\lambda) = \frac{ATN_{OA-sol}(\lambda)}{l} \tag{5}$$

165 where l is the optical path length.

166 The absorbance measurements are aimed at inferring the imaginary part of the refractive index. For this,

167 $b_{abs,OA-sol}(\lambda)$ is transformed to the absorption coefficient of the bulk OA in the pure form, $b_{abs,OA-bulk}$ (Sun et al.,

168 2007):

169 $$b_{abs,OA-bulk}(\lambda) = b_{abs,OA-sol}(\lambda) \left. \rho_{OA} \middle/ \frac{m_{OA}}{V_{solvent}} \right. \tag{6}$$

170 where ρ_{OA} is the bulk density of OA (assumed to be 1.5 g cm^{-3}, typical of wood-burning OA; (Corbin et al., 2015a;

171 Moosmüller et al., 2009; Sun et al., 2007)), m_{OA} is the extracted OA mass, and $V_{solvent}$ is the solvent volume. The

172 bulk absorption coefficient directly leads to the imaginary part of the OA refractive index, k_{OA}, in pure form

173 (Moosmüller et al., 2009):

174 $$k_{\mathrm{OA}}(\lambda) = b_{\mathrm{abs,OA-bulk}}(\lambda)\frac{\lambda}{4\pi} \tag{7}$$

175 Inserting Eq. (6) into Eq. (7) eventually provides (Liu et al., 2015a):

176 $$k_{\mathrm{OA}}(\lambda) = \frac{\lambda\rho_{\mathrm{OA}}V_{\mathrm{solvent}}}{4\pi m_{\mathrm{OA}}} b_{\mathrm{abs,OA-sol}}(\lambda) \tag{8}$$

177 The mass of organics dissolved in the solution could not be quantified. Therefore, we use an upper limit value for

178 m_{OA}, approximated as the integral of AMS-measured OA mass concentration times sample flow rate over the filter-

179 sampling period. Accordingly, the resulting k_{OA} values represent lower limits for the true values, as the OA

180 extraction efficiency was not accounted for. If the OA extraction efficiency was less than unity, then the absorption

181 (or MAC) predicted from our solvent-extraction measurements would be less than that measured (or calculated)

182 using our real-time measurements (MWAA-calibrated aethalometer).

183 **2.3 Uncertainty analysis**

184 It is important to draw a clear distinction between uncertainties related to measurement precision and accuracy and

185 those related with experimental variability. In this section we discuss the quantifiable and unquantifiable

186 uncertainties related with the different measurements. In the result section, we will present our confidence levels on

187 the average parameters determined based on the experimental variability, which we judge to be the main source of

188 variance in the data.

189 **Quantifiable uncertainties.** The estimated uncertainty in the AMS-derived OA mass concentrations is ~25%,

190 which includes both potential biases and precision. This estimate is based on the variation in the AMS calibration

191 factors and estimated uncertainties in the SMPS used for the AMS calibration (Bruns et al., 2015, 2016).

192 Uncertainties related to particle transmission efficiency in the AMS are considered negligible for the particles

193 sampled here (Liu et al., 2007), whose volume size distribution falls within the range transmitted efficiently by the

194 AMS aerodynamic lens (see Fig. S4). The bounce-related collection efficiency (CE) of the AMS was concluded to

195 be unity for wood-burning OA in the literature reviewed by Corbin et al. (2015b; in their Section S1.2). For the

196 present data, the comparison between the SMPS mass (predicted from fitted volume distributions using a density of

197 1.5 g cm^{-3}) and the total PM predicted as AMS-OA+eBC, suggest a CE value between 0.7 and 1.0 (19% relative

198 uncertainty), consistent with average literature values and the uncertainties estimates. The uncertainty in EC mass

199 concentration, estimated from measurement repeats based on the EUSAAR2 protocol only, is within 7% in our case.

The precision uncertainty in the aethalometer attenuation measurements was estimated as 15 Mm^{-1} based on the standard deviation of its signals prior to aerosol being injected into the smog chamber. The MWAA data have an estimated noise level and precision of 12 /Mm and 10% respectively, and these uncertainties have been added in quadrature to provide the overall uncertainties shown, for example, as error bars in Fig. 1 below. To compare the MWAA and aethalometer measurements, we determined $b_{abs,MWAA,880nm}$ by extrapolating the absorption coefficients measured at 850 nm to 880 nm using an α-value determined from the ratio between the absorption coefficients at 850 nm and 635nm. The uncertainty associated with this extrapolation is considered negligible relative to the overall MWAA uncertainty.

Possible unquantified uncertainties. There are significant uncertainties in the measurement of aerosol absorption using filter-based techniques (e.g., Collaud Coen et al., 2010). Here, we have used MWAA measurements as a reference to scale the aethalometer data, using a single C value. The correction factor C, which accounts for scattering effects within the filter matrix (Drinovec et al., 2015), may depend on the aerosol sample (Collaud Coen et al., 2010). In this study, we evaluated the variability in this factor for our primary and aged samples, by directly comparing the aethalometer to MWAA measurements, as discussed below. The MWAA has been previously validated against a polar nephelometer and a MAAP (Massabo et al., 2013), which, in turn, has been validated against numerous in situ methods (e.g., Slowik et al., 2007). The excellent correlation between MWAA and EC in our study (discussed below) supports the high confidence in the MWAA filter based absorption measurements conducted here. Another significant source of uncertainty in filter-based absorption measurements is the possible sorption (or evaporation) of volatile organics on (or from) the filter material. This may lead to an overestimation (or underestimation) of OA absorption. However, we have minimized sorption artefacts by utilizing a charcoal denuder. We have obtained an excellent correlation between OA absorption measurements derived from the MWAA-calibrated aethalometer and from quartz filter samples (see discussion below, Fig. 6 in the main text and S13 in the supplementary information). Although both of these techniques involved filter sampling, their sampling timescale is an order of magnitude different, and a difference is therefore expected if sorption (or evaporation) caused a substantial bias in our results. We therefore conclude that it is unlikely that artifacts associated with filter sampling have biased the absorption measurements. Finally, uncertainties related to pyrolysis during thermo-optical analysis may bias EC measurements. Such uncertainties arise from unstable organic compounds, and can be significant for biomass-burning samples, leading to biases on the order of 20% for EC (e.g. Schauer et al., 2003; Yang and Yu., 2007). To minimize these biases we applied the EUSAAR2 protocol. The optical properties of such organics are

229 generally different from BC; therefore, the excellent correlation between MWAA and EC data in Fig. 1A suggest

230 that pyrolysis effects were not a major source of uncertainty in our data set.

231

232   **3.   OPTICAL PROPERTIES ANALYSIS**

233 **3.1 Determination of absorption Ångström exponents and mass absorption cross-sections**

234 In this section we describe the methodology adapted for the determination of the mass absorption cross-sections

235 (MACs) for the different aerosol material from the Sunset, MWAA and aethalometer measurements. The

236 assumptions and limitations underlying these calculations are clearly stated. We also explain the relationship

237 between the MACs and the wavelength dependence of the overall absorption.

238 **Definition of the absorption Ångström exponent .** The wavelength dependence of the overall absorption due to

239 both BC and BrC has often been described assuming a power law:

240    $$b_{abs}(\lambda) \propto \lambda^{-\alpha} \qquad\qquad (9)$$

241 where α is the Ångström absorption exponent, often determined by fitting the absorption coefficient measurements

242 across the entire wavelength range. Eq. (9) is an empirical simplification, which breaks down when different

243 components having different spectral dependence contribute to the absorption, e.g. a mix of BrC and black carbon

244 (e.g., Moosmüller et al., 2011). In practice, different values of α would be obtained for different choices of λ ranges,

245 and therefore we alternatively calculated two-wavelength absorption exponents according to

246    $$\alpha(\lambda, \lambda_{ref}) = -\frac{\ln\left(\dfrac{b_{abs}(\lambda)}{b_{abs}(\lambda_{ref})}\right)}{\ln\left(\dfrac{\lambda}{\lambda_{ref}}\right)} \qquad\qquad (10)$$

247 where λ is a wavelength of interest (in nm) and λ_{ref} is the reference wavelength, here 880 nm. This reference

248 wavelength was chosen, because BC is expected to fully dominate light absorption in this range (Laskin et al.,

249 2015).

250 Black carbon is known to have an α between 0.9 and 1.1 (Bond et al., 2013; Kirchstetter et al., 2004; Liu et al.,

251 2015b), whereas BrC, which preferentially absorbs at shorter wavelength, has a higher α (Laskin et al., 2015; Saleh

252 et al., 2013). Thus, we interpret an increase of $\alpha(\lambda, \lambda_{ref})$ of the total aerosol as due to an increased contribution of

253 BrC to the total absorption. $\alpha(\lambda, \lambda_{ref})$ can potentially change due to other effects such as a wavelength dependent

254 lensing effect on absorption by BC (e.g., Lack and Langridge, 2013) or the restructuring of BC aggregates during

255 aging. The former effect was negligible under our conditions, as elaborated on below. The latter, if it occurs during

256 aging, would be attributed to SOA absorption in our approach. However, this is not an issue if our values are

257 accordingly applied in e.g. model simulations, following the same assumption as in our approach. This means that

258 the potential restructuring effects must implicitly be considered within the MAC(λ) of SOA, while the MAC(λ) of

259 BC must be kept fixed.

260 **3.2 Determination of MAC$_{BC}$ and MAC$_{POA}$ using the absorption Ångström exponent**

261 In a mixture of n absorbing species, the total absorption at any wavelength may be written as the sum of the

262 absorbance of each of the species. Accordingly, Eq. (10) can be expressed for a multi-component system

263 $$\alpha(\lambda, \lambda_{\text{ref}}) = \frac{1}{\ln(\lambda_{ref}/\lambda)} \ln\left(\frac{\sum_{i=1}^{n} b_{\text{abs,i}}(\lambda)}{\sum_{i=1}^{n} b_{\text{abs,i}}(\lambda_{ref})}\right) = \frac{1}{\ln(\lambda_{ref}/\lambda)} \ln\left(\frac{\sum_{i=1}^{n} M_i MAC_i(\lambda)}{\sum_{i=1}^{n} M_i MAC_i(\lambda_{ref})}\right) \quad (11)$$

264 where the right hand side follows the general definition of MAC along the lines of Eq. (4). M_i and MAC$_i$ are the

265 mass concentration and MAC, respectively, of the ith species, with n absorbing species in total. By considering that

266 the light absorption at λ_{ref} = 880 nm is exclusively due to BC, and by defining BC to be the nth species, Eq. (11)

267 can be written as

268 $$\alpha(\lambda, 880nm) = \frac{1}{ln(880nm/\lambda)} ln\left(\frac{MAC_{BC}(\lambda)}{MAC_{BC}(880nm)} + \sum_{i=1}^{n-1} \frac{M_i MAC_i(\lambda)}{b_{\text{abs}}(880nm)}\right) \quad (12)$$

269 In Eq. (12), the summation now only goes over the n-1 organic species, which contribute to light absorption.

270 The fresh combustion aerosol exclusively contains BC and POA as absorbing species. For the data at time t_0 before

271 the start of photo-oxidative aging, Eq. (12) simplifies to:

272 $$\alpha(t_0, \lambda, 880nm) = \alpha_{\text{BC+POA}}(t_0, \lambda, 880nm)$$

273 $$= \frac{1}{\ln(880\text{nm}/\lambda)} \ln\left(\frac{\text{MAC}_{\text{BC}}(t_0,\lambda)}{\text{MAC}_{\text{BC}}(t_0,880nm)} + \frac{M_{\text{OA}}(t_0)\text{MAC}_{\text{POA}}(t_0,\lambda)}{b_{\text{abs}}(t_0,880nm)}\right)$$ (13)

274 In Eq. (13), $M_{\text{OA}}(t_0)$ is the mass concentration of primary organic aerosol measured by the AMS at t_0.

275 $\text{MAC}_{\text{BC}}(t_0,880\text{nm})$ was inferred from the MWAA and Sunset thermo-optical analysis and shown to be independent

276 of the experimental conditions (Section 4.1; Fig. 1A). Absorption coefficients $b_{\text{abs}}(t_0,\lambda)$ are obtained from the high

277 time resolution attenuation measurements by the aethalometer referenced to the MWAA absorption measurements

278 as described above. $\alpha(t_0,\lambda,880\text{ nm})$ is derived from $b_{\text{abs}}(t_0,\lambda)$ and $b_{\text{abs}}(t_0,880\text{ nm})$ using Eq. (10). We have

279 intentionally formulated of Eq. (13) as such to highlight that the retrieved $\text{MAC}_{\text{OA}}(t,\lambda)$ depends mainly on the input

280 $M_{\text{OA}}.$ Correspondingly, the retrieved $\text{MAC}_{\text{OA}}(t,\lambda)$ is mainly sensitive to potential AMS calibration biases. This leaves

281 only 2 free parameters in Eq. (13), $\text{MAC}_{\text{BC}}(t_0,\lambda)$ and $\text{MAC}_{\text{POA}}(t_0,\lambda)$. These were determined by fitting Eq. (13) to

282 $\alpha(t_0,\lambda,880\text{ nm})$, $M_{\text{OA}}(t_0)$, $\text{MAC}_{\text{BC}}(t_0,880\text{nm})$ and $b_{\text{abs}}(t_0,880nm)$ data measured in all experiments for fresh

283 emissions at t_0. This approach contains the implicit assumption that the two MAC values are also independent of

284 experimental conditions, and therefore these MACs should be considered as average values. The accuracy of these

285 MAC values obviously depends on the accuracy of the absorption and mass measurements. First, a systematic bias

286 in the C value potentially caused by a systematic bias in the MWAA measurements propagates to an identical bias in

287 both $\text{MAC}_{\text{BC}}(t_0, \lambda)$ and $\text{MAC}_{\text{POA}}(t_0, \lambda)$. Second, a systematic bias in the Sunset EC mass measurements yields a

288 corresponding inverse bias in $\text{MAC}_{\text{BC}}(t_0, \lambda)$, while $\text{MAC}_{\text{POA}}(t_0, \lambda)$ remains unaffected. Third, a systematic bias in the

289 AMS POA mass yields a corresponding inverse bias in $\text{MAC}_{\text{POA}}(t_0, \lambda)$, while $\text{MAC}_{\text{BC}}(t_0, \lambda)$ remains unaffected. Eq.

290 (13) shows that α of the primary aerosol at a certain wavelength is largely driven by $\text{MAC}_{\text{POA}}(t_0, \lambda)$, i.e. the optical

291 properties of POA, and by the ratio $\frac{M_{\text{OA}}(t_0)}{b_{\text{abs}}(t_0,880nm)}$, which reflects the relative contributions of POA and BC to total

292 primary aerosol mass.

293 **3.3 Determination of MAC_{SOA}**

294 The MAC of SOA, MAC_{SOA}, can be generally defined as:

295 $$\text{MAC}_{\text{SOA}} = \frac{b_{\text{abs,SOA}}}{M_{\text{SOA}}}$$ (14)

296 where $b_{\text{abs,SOA}}$ and M_{SOA} are the absorption coefficient and mass concentration of SOA, respectively. In the aged

297 aerosol, which contains the absorbing species BC, POA and SOA, $b_{\text{abs,SOA}}$ is the difference of the total absorption

298 minus the absorption by POA and BC:

12

299     $b_{\text{abs,SOA}}(t,\lambda) = b_{\text{abs}}(t,\lambda) - b_{\text{abs,POA+BC}}(t,\lambda)$ (15)

300   The absorption by POA and BC in the aged aerosol is a priori unknown, but can be calculated under certain

301   assumptions. The first assumption is that SOA does not contribute to absorption at 880 nm:

302     $b_{\text{abs,POA+BC}}(t, 880\,nm) \equiv b_{\text{abs}}(t, 880\,nm)$. The second assumption is that the two-λ α values of primary emissions

303   do not change during aging $\alpha_{\text{POA+BC}}(t,\lambda, 880\,nm) \equiv \alpha_{\text{POA+BC}}(t_0,\lambda, 880\,nm)$. The latter approximation is based on

304   the underlying assumptions that the MAC of POA is not altered by aging and that the proportions of POA and BC

305   mass lost to the wall are identical. Under these assumptions $b_{\text{abs,POA+BC}}$ becomes:

306     $b_{\text{abs,POA+BC}}(t,\lambda) = b_{\text{abs}}(t, 880\,nm)\left(\frac{880\,nm}{\lambda}\right)^{\alpha_{\text{POA+BC}}(t_0,\lambda,880\,nm)}$ (16)

307   Note that inferring $b_{\text{abs,POA+BC}}(t,\lambda)$ from $b_{\text{abs}}(t, 880\,nm)$ implicitly accounts for the decrease in the BC and POA

308   absorption due to wall losses.

309   M_{SOA} was obtained as total organic minus POA mass concentration:

310     $M_{\text{SOA}}(t) = M_{\text{OA}}(t) - M_{\text{POA}}(t)$ (17)

311   The POA mass concentration in the aged aerosol can be inferred from the initial OA mass concentration in the fresh

312   emissions by accounting for the wall losses using Eq. (S1) and the wall loss time constant τ (see Section Wall loss

313   corrections in the SI):

314     $M_{\text{POA}}(t) = M_{\text{OA}}(t_0)\exp(\tau^{-1}t)$ (18)

315   Inserting Eq. (15) - (18) into Eq. (14) provides the final equation for inferring MAC_{SOA}.

316     $\text{MAC}_{\text{SOA}}(t,\lambda) = \dfrac{b_{\text{abs}}(t,\lambda) - b_{\text{abs}}(t, 880\,nm)\left(\frac{880\,nm}{\lambda}\right)^{\alpha_{\text{POA+BC}}(t_0,\lambda,880\,nm)}}{M_{\text{OA}}(t) - M_{\text{OA}}(t_0)\exp(\tau^{-1}t)}$ (19)

317

318   MAC_{SOA} can be calculated for every data point in time and for all aethalometer wavelengths from 370 to 660 nm

319   (MAC_{SOA} defined to be zero at $\lambda \geq 880$ nm), as all quantities on the right hand side of Eq. (19) are available from

320   either the aethalometer or AMS measurements or are otherwise known. It can be seen from Eq. (19) that the mass

321   concentrations used to calculate MAC_{SOA} solely originate from AMS data, thus being consistent with the calculation

322   of MAC_{POA} (see above). Eq. (19) is based on the assumption that POA is "chemically inert", i.e. no chemically

13

323   induced changes of M_{POA} and MAC_{POA} occur. Such chemically induced changes of absorption coefficient by POA,

324   through a change of M_{POA} or MAC_{POA}, if they occur, are assigned to the absorption by SOA, thus resulting in a

325   corresponding adjustment of the inferred MAC_{SOA}.

326   **3.4 Mie calculation to relate k_{OA} with MAC_{OA}**

327   The imaginary part of the refractive index of an aerosol component is an intensive material property. However, the

328   MAC of such an aerosol component additionally depends on the size and morphology of the aerosol (except for the

329   Rayleigh regime). The online aerosol absorption measurements provide estimates for MAC values, while the UV-

330   visible absorbance measurements of filter extracts provide the imaginary part of the refractive index. We used Mie

331   calculations in order to compare the two quantities. The $k_{OA}(\lambda)$ obtained from the filter extracts is converted to a

332    $MAC_{OA,bulk}$ by assuming that all OA is present in homogeneous spherical particles with a diameter distribution

333   identical to the mobility diameter distribution measured by the SMPS. In this manner, $MAC_{OA,bulk}$ becomes equal to

334   the mass-weighted average (=volume-weighted average) of the diameter dependent MAC:

335    $$MAC_{OA,bulk}(\lambda, n_{OA}, k_{OA}, \rho_{OA}) = \frac{\sum_i N_i d_i^3 MAC_i^{Mie}(\lambda, n_{OA}, k_{OA}, \rho_{OA})}{\sum_i N_i d_i^3} \qquad (20)$$

336   Here, N_i and d_i are the number of particles and particle diameter, respectively, in the ith size bin, and n_{OA} is the real

337   part of the refractive index of the OA (which is assumed to be $n_{OA} = 1.5$ typical for organic material; Lu et al.,

338   2015). The MAC of particles with diameter d_i, MAC_i^{Mie}, was calculated using the Mie Code by Peña and Pal (2009)

339   (incorporated into Igor Pro 6.3, WaveMetrics, OR, USA by Taylor et al., 2015). MAC_i^{Mie} also depends on the density

340   of OA, for which we assume a value of $\rho_{OA} = 1.5$ g cm^{-3} (see Section 2.2), as the volume specific absorption cross-

341   section obtained from Mie theory needs to be converted to a mass specific absorption cross-section. We note that as

342   we have used the same value of ρ_{OA} in the calculation of both MAC_i^{Mie} and $k_{OA}(\lambda)$, $MAC_{OA,bulk}$ becomes

343   independent of the assumed ρ_{OA} value.

344   Assuming spherical particles and neglecting the presence of BC in these particles may seem inappropriate. However,

345   calculations considering BC and assuming core-shell morphology revealed (1) limited sensitivity of the resulting

346   MAC_{OA} to this assumption and (2) a higher than measured lensing effect. Therefore, a substantial fraction of the OA

347   seems to be externally mixed and to dominate the measured size distribution (see also Section 4.1).

348

4. RESULTS AND DISCUSSION

4.1 Verification of MAC_{BC} and C value

349

350

351 We have independently determined the MAC_{BC}(880nm) and the aethalometer C values under our conditions, as

352 follows. We determined MAC_{BC}(880nm) from the regression between the absorption coefficients at 880 nm

353 obtained from the MWAA and the EC mass measured by the Sunset analyzer (Fig. 1A). The slope of this regression

354 may be used to estimate the MAC_{BC}(880nm), which we retrieved as 4.7 ± 0.3 m^2g^{-1} by an uncertainty-weighted

355 linear least-squares fit . The corresponding intercept was not significantly different from zero (-3 ± 3 /Mm). Our

356 MAC_{BC}(880nm) is not statistically significantly different from the value recommended by Bond et al., (2006) for

357 externally-mixed BC (extrapolating their MAC_{BC}(550nm) to 880 nm by assuming α=1 provides MAC_{BC}(880nm)=

358 4.7 ± 0.7 m^2g^{-1}). The strong correlation between $b_{abs,MWAA,880nm}$ and EC in Fig. 1A shows that MAC_{BC}(880nm) did

359 not vary with aging during our study (see also Fig. S2-a). It also indicates that measurement artefacts for both

360 instruments were negligible, as the fundamental differences between the two techniques mean that any artefacts are

361 unlikely to be similar between them (charring for EC vs. adsorption artefacts for MWAA). Our absorption

362 coefficient measurements also provide insights into particle mixing state in this study. Since a single MAC

363 adequately described our samples at all levels of aging (Fig. 1A and Fig. S2-a), in spite of a factor of 3.3 average

364 increase in the aerosol mass, our samples cannot be adequately described by a core-shell Mie model. Such a core-

365 shell model would predict an absorption enhancement by a factor of ~1.8 (Bond et al., 2006) for the observed OA

366 mass increase with aging, which was not observed in our case. This observation is also supported by the time

367 resolved attenuation measurements at 880 nm using the aethalometer (Fig. S3), suggesting that little (<10%) to no

368 increase in the attenuation coefficients upon SOA formation. We emphasize that this conclusion does not indicate

369 that no internal mixing occurred, but rather that the simplified concept of negligible mixing better describes our data

370 than the equally simplified concept of a core-shell description of coatings that completely envelop the central BC

371 core. This may be due to the complex morphology of internally-mixed BC, which has been previously observed for

372 wood burning particles (e.g., China et al., 2013; Liu et al., 2015; Liu et al., 2017). It may also be related to the fact

373 that OA and BC are emitted during separate phases of combustion. OA rich particles are emitted during the pre-

374 flaming pyrolysis stage of combustion, whereas most BC is emitted during flaming combustion (Corbin et al.,

375 2015a, 2015b; Haslett et al., 2018; Heringa et al., 2011). These two stages of combustion may coexist in different

376 regions of the stove, particularly during simulated real-world usage. As lensing effect was negligible in our case, we

377 have assumed that the aerosol optically behaves as an external mix between BC and BrC during Mie calculation (see

378 section 3.4). We note that while this assumption is important for estimating the BC absorption, the conclusion drawn

379 about the BrC absorption are not very sensitive to the assumed morphology.

380 We determined time-resolved wavelength-dependent absorption coefficients as follows. We used the aethalometer to

381 obtain filter attenuation coefficients with high time resolution, which were then calibrated to obtain absorption

382 coefficients by deriving the factor C (Eq. (1)) using the MWAA measurements of filter samples. C was obtained

383 from an uncertainty-weighted linear least-squares fit as 3.0 ± 0.2 (Fig. 1B); the intercept of the fit was not

384 significantly different from zero, within two standard deviations (-17 ± 14). A very strong correlation could be

385 observed between MWAA and aethalometer (Fig. 1B), implying that C is independent of the type of the aerosol

386 sampled (see also Fig. S2-B). Therefore, we used a single C value to obtain time-resolved wavelength-dependent

387 absorption coefficients from the aethalometer attenuation measurements at the different wavelengths for primary and

388 aged aerosols.

389 Note that the manufacturer's default values, which were not applied in our case, are 1.57 for C (using TFE-coated

390 glass fiber filters) and 12.2 m^2 g^{-1} for σ_{ATN} at 880 nm (Gundel et al., 1984 , Drinovec et al., 2015). The C value

391 determined here is larger than the manufacturer-default value for the AE33, resulting in smaller absorption

392 coefficients. However, the calculated σ_{ATN} at 880 nm (13.8 m^2 g^{-1}), which can be retrieved as the product of the C

393 value and $MAC_{BC}(880nm)$ (Eq. (3)), is similar to the factory-default σ_{ATN}. Therefore, our calibrated M_{eBC}, calculated

394 from the attenuation coefficients using σ_{ATN} (Eq. (2)), are similar to the factory-default M_{eBC}. We note that M_{eBC} has

395 not been used for MAC_{OA} calculations, and is only used for the calculation of the mass fractions of BC and OA for

396 display purposes (Fig. 2, 3, 7 and 8).

397 **4.2 Optical properties of BC, POA, and SOA**

398 In this section we derive the wavelength dependent mass absorption cross-sections for BC, POA and SOA. In Fig. 2,

399 we display the evolution of $\alpha(370nm, 880nm)$ as a function of OH exposure. Fig. 3 shows the relationship between

400 $\alpha(\lambda, 880nm)$ and f_{OA} for primary and aged aerosols.

401 **α of primary emissions.** The $\alpha(370nm, 880nm)$ values computed for the primary aerosol (OH exposure = 0

402 molecules cm^{-3} h) ranged between 1.3 and 1.7 (Fig. S5), which is within the range reported previously for biomass-

403 burning emissions (Kirchstetter et al., 2004; Lewis et al., 2008; Zotter et al., 2016). The $\alpha(\lambda, 880nm)$ is slightly

404 higher than that of pure BC (~1.2; Bond et al., 2013; Zotter et al., 2017) for small f_{POA}, while increasing f_{POA}

405 corresponded to a distinct increase of $\alpha(\lambda, 880nm)$. This increase provides clear evidence for the contribution of

406 primary BrC to the absorption at lower wavelengths (shown explicitly in Eq. (13)). The f_{POA} ranges from 0.12 to

407 0.63, which is lower than f_{POA} reported for open burning emissions (e.g., f_{POA}~0.75, Ulevicius et al (2016)), because

408 our wood-stove emissions feature a more efficient combustion. As illustrated in Fig. S5, the observed absorption

409 spectra have steeper gradients with decreasing wavelength compared to the lines of constant α. Such systematic

410 increase in $\alpha(\lambda, 880nm)$ with decreasing λ reflects the more-efficient light absorption by BrC at shorter wavelengths

411 (Moosmüller et al., 2011), and shows that the power law wavelength dependence is an inaccurate oversimplification

412 for this mixed aerosol.

413 **Evolution of α with aging.** Fig. 3B shows that upon aging, the OA fraction rapidly increased (a typical time series

414 of raw data is shown in Fig. S1), reaching an average value of 0.81 (full range for aged OA: $0.74 < f_{OA} < 0.89$) at

415 high OH exposures ($> 2{\times}10^7$ molecules cm^{-3} h), and resulting in a corresponding increase of

416 $\alpha_{BC+POA+SOA}(370nm, 880nm)$. The increase of $\alpha_{BC+POA+SOA}(370nm, 880nm)$ and f_{OA} were always correlated

417 and plateaued at OH exposures beyond ~$2{\times}10^7$ molecules cm^{-3} h, as seen in Fig 2. Also, note in Fig. 2 that at highest

418 OH exposures, the highest $\alpha_{BC+POA+SOA}(370nm, 880nm)$ were reached, on average 1.8, during experiments where the

419 f_{OA} was highest. Such strong correlation between SOA formation and $\alpha_{BC+POA+SOA}(370nm, 880nm)$ suggests the

420 production of substantial amounts of brown SOA. A similar relationship is observed between

421 $\alpha_{BC+POA+SOA}(\lambda, 880nm)$ and f_{OA} for higher wavelengths as shown in Fig. S6. Similar to the case of POA, a

422 systematic decrease in $\alpha(\lambda, 880nm)$ with increasing λ is observed, reflecting the preferential absorption of BrC

423 SOA at shorter wavelengths. We note that $\alpha_{BC+POA+SOA}(370nm, 880nm)$ as a function of f_{OA} for all experiments

424 lies below the overall trend for the primary aerosol (dashed line in Fig. 3B), implying that MAC$_{SOA}$(370nm) was

425 smaller than MAC$_{POA}$(370nm).

426 **Determination of MAC$_{BC}$ and MAC$_{POA}$.** We determined best-fit values for MAC$_{BC}(\lambda)$ and MAC$_{POA}(\lambda)$ from the

427 data shown in Fig. 3A. Fig. 3A includes least-squares fits of Eq. (13) to the data, with MAC$_{BC}(\lambda)$ and MAC$_{POA}(\lambda)$ as

428 fit parameters. The fit results are shown in Table 1. The obtained fit value of MAC$_{BC}$(370nm) was 13.7 m^2 g^{-1} (GSD

429 1.1, one-sigma uncertainty 12.4—15.1 m^2/g), higher but not statistically significantly different from the range

430 estimated based on Bond et al. (2013), considering the uncertainties on both the α_{BC} values and the MAC$_{BC}$(520nm).

431   Meanwhile, the mean MAC_{POA}(370nm) value, equal to 5.5 m^2 g^{-1}, obtained under our conditions for domestic wood

432   burning is ~2.4 times higher than that obtained by Saleh et al. (2014) for open biomass burning primary emissions,

433   suggesting the presence of more-strongly absorbing organic material under our conditions (this comparison is

434   continued in Section 4.3).

435   **Determination of MAC_{SOA}.** The $MAC_{SOA}(\lambda)$ values, determined using Eq. (19), are shown in Fig. 4 and Table 1.

436   MAC_{SOA}(370nm) was 2.2 m^2 g^{-1} (GSD 1.39), a factor of 2.5 smaller than MAC_{POA}(370nm), but approximately an

437   order of magnitude higher than values reported for ambient oxygenated aerosols or laboratory SOA from biogenic

438   and traditional anthropogenic precursors such as terpenes and methyl-benzenes (Clarke et al., 2007; Lambe et al.,

439   2013; Liu et al., 2016; Romonosky et al., 2015). The predominant SOA precursors identified in wood smoke

440   comprise (methyl)naphthalene(s) and phenol derivatives from lignin pyrolysis (Bruns et al., 2016; Ciarelli et al.,

441   2016), the oxidation products of which are expected to be highly light absorbing due to the presence of aromatic

442   moieties in the SOA (Bruns et al., 2016; Laskin et al., 2015). In this regard, it is not surprising that the

443   MAC_{SOA}(370nm) values obtained here are similarly high as those obtained from methanol-extracted SOA from

444   guaiacol and naphthalene oxidation (0.5–3.0 m^2 g^{-1}, Romonosky et al., 2015).

445   **Uncertainties and variability in MAC_{BC}, MAC_{POA} and MAC_{SOA}.**

446   Table 1 shows the fitting errors related with $MAC_{BC}(\lambda)$, $MAC_{POA}(\lambda)$ and $MAC_{SOA}(\lambda)$, arising from our

447   measurement precision and experimental variability. These fitting errors are greater than our estimated uncertainties

448   in the absorption coefficients measured by MWAA (10%), and comparable to our estimated uncertainty in OA mass

449   measured by AMS (30%). The residuals in the fitted $MAC_{BC}(\lambda)$ are relatively low (< 10%), increasing with

450   decreasing λ. By contrast, the uncertainties in the fitted $MAC_{POA}(\lambda)$ are much higher (GSD = 1.2–1.5) and increase

451   with increasing λ. The relative residuals between the measured and fitted $\alpha(\lambda,880nm)$ for primary emissions showed

452   a mean bias and RMSE of 0.07 and 0.13, respectively (Fig. S7), indicating that our fitted MAC results provide a

453   good description of the data set. $MAC_{SOA}(\lambda)$ values determined were highly variable between experiments with a

454   GSD = 1.39 and 2.42 for λ=370 nm and 660 nm, respectively. In Fig. S10, we show the distribution of $MAC_{SOA}(\lambda)$

455   values as box and whiskers against OH exposure, showing no particular dependence of these values with aging as it

456   will be discussed below. Therefore, we expect the fitting errors in MAC_{SOA} and of MAC_{POA} to be mainly related to

457   true changes in the organic aerosol chemical composition between different burns, since the variability of $MAC_{BC}(\lambda)$

458 was relatively small. In Section 4.3, we discuss this variability further using the results of an additional and

459 independent analysis.

460 **MAC$_{BC}$, MAC$_{POA}$ and MAC$_{SOA}$ wavelength dependence.** The relationships between the MAC$_{SOA}(\lambda)$, MAC$_{POA}(\lambda)$

461 and MAC$_{BC}(\lambda)$ and wavelength appear to fall on three unique lines in the range 660 nm to 370 nm when plotted in

462 log-log space, as shown in Fig. 4 (Fig. S8 shows the same data plotted on a linear scale). This indicates that a power-

463 law approximation provides a good description of the behavior of individual components within this wavelength

464 range from 370 nm to 660 nm. Accordingly we fitted the power law coefficients to the data shown in Fig. 4

465 ($\ln(MAC_i) = \ln(A_i) + \alpha_i \ln(\lambda)$, with $i=$ BC, POA, or SOA) and fitting parameters are shown as multivariate

466 probability density functions in Fig. S9. This yielded $\alpha_{BC} = 1.2$, $\alpha_{POA} = 4.6$, and $\alpha_{SOA} = 5.6$, with corresponding

467 uncertainties of approximately 20% (complete details of the uncertainties are provided in Table S1). Note that α_{BC} in

468 the range 660 nm to 370 nm obtained from this fit is very similar to α_{BC} values that can be inferred by extrapolating

469 the data shown in Fig. 3A to $f_{OA}=0$. The high α values obtained for the organic fractions are consistent with previous

470 measurements for BrC containing POA (e.g. Chakrabarty et al., 2010, 2013).

471 **Evolution of MAC$_{OA}$ with aging.** In Fig. 5, we examine whether the absorption profile of SOA evolved with aging.

472 A change in MAC$_{SOA}(370nm)$ or α_{SOA} with increasing OH exposure may indicate either a change in the mass-

473 specific absorption of the condensing SOA species with time, or a change (e.g. "bleaching") in the MAC of pre-

474 existing POA. Fig. 5 indicates that neither of these scenarios was the case. Both MAC$_{SOA}(370nm)$ and α_{SOA} were

475 statistically independent of the OH exposure, for exposures up to 40 molec. OH cm^{-3} h. This signifies that under our

476 conditions and within our measurement uncertainties the optical properties of the additional organic mass formed

477 was constant with aging, under the assumption that the light-absorption properties of POA were negligibly

478 influenced by aging. Most of the variability in MAC$_{SOA}(\lambda)$ discussed above is therefore related to experiment-to-

479 experiment differences rather than to the extent of OH exposure, as it is also shown below.

480 **4.3 Solubility of BrC in methanol and water**

481 Fig. 6 shows the MAC$_{OA}(370nm)$ determined from the water and methanol extracts against the MAC$_{OA}(370nm)$

482 determined from the online measurements. The MAC$_{OA}(370nm)$ from online measurements was estimated by

483 subtracting the contribution of BC assuming a constant MAC$_{BC}(370nm) = 13.7$ m^2.g^{-1} as obtained in this work

484 (Table 1). We performed all the calculations and comparisons at $\lambda = 370$ nm, as the signal to noise ratio of the

485 absorption coefficients measured by UV-visible spectroscopy and the contribution of BrC to the total carbonaceous

486   absorption are highest at this wavelength. The MAC of the extracts was computed from the k_{OA} through Mie

487   calculations. Repetition of both water and methanol extracts yielded results that were consistent within 10% (Fig.

488   S11). Average raw absorption spectra are shown in Fig. S12.

489   Fig. 6B shows excellent correlation between the MAC_{OA}(370nm) values obtained from the kOA of the solvent-

490   extracted OA with the in-situ method described above. The Pearson correlation coefficient was 0.8, for both

491   solvents. This correlation suggests that none of the assumptions employed in either method led to substantial errors

492   in precision, providing direct support for our results. A similar relationship was observed between k_{OA} and the

493   MAC_{OA}(370nm) determined from the online measurements (Fig. S13), showing that this relationship is not sensitive

494   to assumptions underlying the Mie calculations. It further suggests that the wide variability observed in the MAC_{OA}

495   values of different burns, as seen Fig. 6, most likely reflects real variability in the optical properties of POA and

496   SOA rather than random noise or experimental errors in the retrieved quantities. MAC_{OA} retrieved based on the k_{OA}

497   of the water soluble OA show substantially more scatter than observed in Fig. 6B (for both primary and aged data),

498   suggesting a variable extraction efficiency in the case of water, which we also attribute to variability in the OA

499   composition.

500   The data in Fig. 6B show that the methanol extracts correspond to a MAC about 50% smaller than the online data.

501   The scatter in the data is significantly reduced for the aged data (note that, in this analysis, aged OA refers to the

502   sum of POA and SOA, since the reported values represent all OA after aging). This reduced scatter is expected,

503   considering that aging is likely to result in more-spherical particles. We have assumed particle sphericity when

504   interpreting the SMPS data and performing the Mie analysis. While the propagation of quantifiable uncertainties

505   leads to an error estimate of ~25%, considering the simplifiations that were necessary for the Mie analysis, we

506   consider a 50% closure to be an adequate agreement. Despite this, we cannot exclude additional methanol insoluble

507   brown carbon. Conversely, the fit in Fig. 6A indicates that the apparent MAC of water-soluble species was a fourth

508   of the respective methanol MAC, according to the slope of only 12 ± 3%. Only the aged data have been fit to

509   illustrate this point. This strong disagreement shows that the BrC in our samples was hardly water soluble, even for

510   the most aged samples. As we expect that the majority of OA in our samples formed by wood pyrolysis (Di Blasi,

511   2008; Corbin et al., 2015b; Shafizadeh, 1984), we can compare our results directly to those of Chen and Bond

512   (2010), who also found that primary wood-pyrolysis BrC was water insoluble. Moreover, the poor water solubility

513   of the light absorbing components of SOA (Zhang et al., 2011) is in line with the results by Bruns et al. (2016) who

514   showed that SOA precursors during these experiments were predominantly aromatic compounds.

515   **4.4 Comparison of k_{OA} with literature**

516   The results above highlight the variability in the OA absorption properties. In this section, we discuss potential

517   reasons for this variability and compare our results to literature. Fig. 7 shows the imaginary refractive index of

518   methanol-extracted OA at 370 nm, $k_{OA,methanol}$(370nm) (Eq. (8)), as a function of M_{BC}/M_{OA} and aging. The data are

519   plotted against M_{BC}/M_{OA} instead of f_{OA} to allow for a direct comparison with literature (see Fig. S14 for a plot

520   against f_{OA}). An approximately linear trend of $k_{OA,methanol}$(370nm) with M_{BC}/M_{OA} is seen in log space. This aging-

521   independent relationship may be useful in, for example, atmospheric scenarios where wood-burning OA is a

522   dominant aerosol component but its exact degree of aging is unknown. The decrease of M_{BC}/M_{OA} caused by

523   formation of SOA during aging results in a concurrent decrease of $k_{OA,methanol}$(370nm), implying that $k_{SOA} < k_{POA}$.

524   This result is consistent with the smaller MAC of SOA compared to POA obtained from online measurements

525   (Table 1) and with recent results reported by Sumlin et al. (2017) . We emphasize that the derived quantity here is

526   the imaginary refractive index k of the total aged OA, not the SOA.

527   The increase of $k_{OA,methanol}$(370nm) with increasing M_{BC}/M_{OA} indicates that the OA compounds present at higher

528   M_{BC}/M_{OA} absorbed more efficiently than at low M_{BC}/M_{OA}. If the variability in M_{BC}/M_{OA} was driven partly by OA

529   partitioning, then this implies that lower-volatility compounds were more absorbing than high-volatility compounds,

530   consistent with the results by Saleh et al. (2014) who investigated the relation between OA absorption and volatility

531   using thermodesorber measurements. A correlation between k_{OA} and M_{BC}/M_{OA} has also been reported by Lu et al.

532   (2015). The parameterizations reported by these authors are included in Fig. 7, where the wavelength dependence

533   reported by those authors has been used to adjust their parameterizations to 370nm. Despite these differences, our

534   results confirm the generality of the correlation proposed by Saleh et al. (2014), but using a method that is

535   independent of potential biases related to internal mixing effects, filter-based absorption measurements or Mie

536   calculations. Indeed, we emphasize that the k_{OA} obtained here is a lower limit: as our approach does not account for

537   the OA extraction efficiency; $k_{OA,methanol}$(370nm) may be underestimated by up to a factor of ~2, based on Fig. 6B.

538

539

540

5. ATMOSPHERIC IMPLICATIONS

541

542 In this section, we seek to estimate the relative importance of OA absorption at different wavelengths relative to that

543 of the total carbonaceous aerosol as a function of aging. For these calculations, the MAC(λ) values for the different

544 components and their relative mass abundance are required. We used the power law parameters reported above to

545 generate continuous $MAC_{BC}(\lambda)$, $MAC_{POA}(\lambda)$, and $MAC_{SOA}(\lambda)$ functions together with their associated uncertainties

546 (Fig. 8A), which allow the extrapolation of these parameters in the range [280nm; 880nm].

547 The contributions of the different components as a function of OH exposure were calculated by assuming that SOA

548 production follows the first order decay of its precursors, i.e., the reaction with OH. Under this assumption, the time-

549 dependent mass concentration of SOA compared to POA can be expressed as

550 $$M_{SOA,WLC}(t)/M_{POA,WLC}(t) = M_{SOAP,WLC}/M_{POA,WLC} \times \left(1 - \exp(-k_{OH}OH_{exp})\right) \qquad (21)$$

551 In this equation, $M_{SOA,WLC}(t)$, $M_{POA,WLC}(t)$ and $M_{SOAP,WLC}$ are the wall loss corrected mass concentrations of SOA,

552 POA and the SOA potential (the maximum SOA formed upon the consumption of all precursors). k_{OH} represents an

553 estimation of reaction rate of SOA precursors towards OH based on SOA production rates. By fitting the observed

554 $M_{SOA,WLC}(t)/M_{POA,WLC}(t)$ against the OH exposure, k_{OH} and $M_{SOAP,WLC}/M_{POA,WLC}$ can be estimated. For these

555 calculations, we have estimated the wall losses using two approaches as described in the SI.

556 The $M_{SOAP,WLC}/M_{POA,WLC}$ was on average equal to 7.8 (GSD = 1.4) and kOH was estimated as 2.7×10^{-11} molecule^{-1}

557 cm^3 (GSD = 1.4), consistent with the SOA precursors chemical nature measured (e.g. PAH and phenol derivatives)

558 by a proton-transfer-reaction mass spectrometer (PTR-MS) (Bruns et al., 2016, 2017). These high rates and

559 enhancement ratios indicate the rapid production of SOA.

560   Based on the bulk gas phase measurements of SOA precursors (Bruns et al., 2016), the obtained enhancements are

561 consistent with high bulk SOA yields of ~50%. These high values are not surprising, considering the nature of these

562 gases (e.g. PAH and phenol derivatives), the low temperatures (263 K), and the relatively high concentrations (Aged

563 OA ~100 µg m^{-3}) at which the experiments have been conducted (Bruns et al. 2016).

564 Combining these calculated enhancements with the average contributions of POA in primary emissions, the

565 evolution of f_{OA} with aging was determined and is shown in Fig. 8B. The uncertainties in Fig. 8B (dotted lines)

566 represent one standard deviation on f_{OA} obtained by a Monte Carlo propagation of uncertainties due to experiment-

567 to-experiment variability, fitting errors and wall loss correction errors (see SI). While this calculation represents a

568 simplification of the SOA production mechanisms (the dependence of SOA yields on OH exposures/multigeneration

569 chemistry and OA mass concentrations was neglected), it results in residuals much smaller than the experiment-to-

570 experiment variability. We therefore used these calculations to assess the relative contribution of OA to the total

571 carbonaceous absorption. We show in Fig. 8C that below 400 nm and upon aging, the absorption coefficient of the

572 total organics was at least as high as the one of BC.

573 Using the MAC values of the different components (in $m^2\ g^{-1}$), their abundance (in $g\ m^{-3}$) and the solar irradiance

574 data (S, in $W\ m^{-2}\ nm^{-1}$) calculated at sea level for a cloudless day, the fractional energy transfer due to the BrC light

575 absorption relative to that due to the total carbonaceous aerosol absorption , $W_{OA}(OH_{exp})$, in air masses dominated

576 by residential burning emissions can be determined as

577 $W_{OA}(OH_{exp}) = RET_{OA}(OH_{exp})/RET_{tot}(OH_{exp})$

578 $$= \frac{\int_{300}^{880}\{M_{POA}(OH_{exp}) \times MAC_{POA}(\lambda) + M_{SOA}(OH_{exp}) \times MAC_{SOA}(\lambda)\} \times S(\lambda) \times d\lambda}{\int_{300}^{880}\{M_{BC}(OH_{exp}) \times MAC_{BC}(\lambda) + M_{POA}(OH_{exp}) \times MAC_{POA}(\lambda) + M_{SOA}(OH_{exp}) \times MAC_{SOA}(\lambda)\} \times S(\lambda) \times d\lambda} \qquad (22)$$

579 Here, $RET_{OA}(OH_{exp})$ and $RET_{tot}(OH_{exp})$ denote the rate of energy transfer per volume (in $W\ m^{-3}$) to the air mass in

580 question due to light absorption by OA and the total carbonaceous aerosol, respectively. We note that while

581 $RET_{OA}(OH_{exp})$ and $RET_{tot}(OH_{exp})$ are extensive properties, $W_{OA}(OH_{exp})$ does not depend on the loading or

582 scattering/lensing, provided that scattering/lensing similarly affects BC and OA present in the same air mass (e.g.

583 BC and OA have a similar size distribution).

584 We also note that $W_{OA}(OH_{exp})$ depends on the photon flux, $S(\lambda)$, but we consider this dependence to be trivial

585 compared to the variability in the aerosol emissions and their light absorbing properties (error bars considering these

586 variabilities are shown in Fig. 8D). Errors in W_{OA} were propagated by Monte Carlo simulations using the

587 uncertainties from the estimated MAC values of BC and OA fractions and the variability in f_{OA}. Our sensitivity

588 analysis suggests that the major part of the variance in predicting W_{OA} for primary emissions stems from the

589 variability in the POA mass fraction. In contrast, the SOA mass absorption cross-sections at lower wavelengths are

590 the most critical factor for assessing the relative importance of BrC absorptivity in aged emissions.

591   Fig. 8D shows that the fractional energy transfer to the air mass, W_{OA}, due to the absorption by the primary organic

592   aerosol was around 10% of that of the total carbonaceous aerosol for our samples. This percentage is comparable to

593   that observed by Fu et al. (2012), in spite of f_{OA} in their samples being much higher, because of the high OA MACs

594   in our samples (Table 1). Moreover, with aging, the fraction of OA is enhanced, resulting in a sizeable increase W_{OA},

595   from ~0.1 to ~0.3 (Fig. 8D), highlighting that SOA formation in biomass burning plumes is an atmospherically

596   relevant source of BrC. We note that our data are more representative of flaming conditions. More data are needed

597   on the chemical nature of primary particulate emissions and of the contributing SOA precursors as well as the

598   absorptivity of these primary and secondary products, for better constraining the influence of biomass-burning

599   related BrC on the Earth's climate.

600

601   **6. CONCLUSIONS**

602   We determined wavelength-dependent MAC values of BC, POA and SOA, as well as k_{OA} for methanol and water

603   extracts of fresh and aged OA, for wood-burning emissions through smog-chamber experiments. To our knowledge,

604   this is the first determination of these properties for wood-burning OA. We showed that the MAC_{OA}(370nm) values

605   calculated based on k_{OA} through Mie analysis correlated well with those estimated from online filter based

606   measurements. This correlation between independent MAC measurements supports the quality of both methods.

607   While MAC_{OA}(370nm) values computed based on $k_{OA,methanol}$ were a 2-fold lower than those estimated from online

608   filter based measurements, calculations based on $k_{OA,water}$ could only explain 12% of the measured absorption,

609   suggesting that BrC species in POA and SOA are mostly water insoluble. The MAC_{OA} was found to vary by more

610   than one order of magnitude. Similar to previous reports, this variability could be related to the variability in the

611   ratio of the mass concentrations of BC and OA (M_{BC}/M_{OA}) due to very different mechanisms of oxidative aging and

612   burn-to-burn variability.

613   The MAC_{POA} and MAC_{SOA} determined for wavelengths between 370 and 660 nm followed a power-law dependence

614   on λ with an absorption Ångström exponent of 4.6 and 5.6 for POA and SOA, respectively. In addition to following

615   this power law, the MACs of POA and SOA appeared to be constant for OH exposures up to 40×10^{6} molecules cm^{-}

616   ^{3} h.

617   The mean MAC_{POA}(370nm) obtained under our conditions was 5.5 m^{2} g^{-1}, considerably higher than previously

reported values for open biomass burning. The mean MAC_{SOA}(370nm) was 2.2 $m^2\,g^{-1}$ (one-sigma variability: 1.6 –

3.1 $m^2\,g^{-1}$ according to a GSD = 1.39) under our experimental conditions, 2.3 times lower than the mean

MAC_{POA}(370nm) but approximately an order of magnitude higher than MAC values estimated for ambient

oxygenated aerosols or reported for SOA from biogenic and traditional anthropogenic precursors. We propose that

the important role of oxidized phenols and aromatics in forming wood-burning SOA (Bruns et al., 2016) is the cause

of this observation. This hypothesis is supported by our observed reaction rates with OH, and by the water-

insolubility of the BrC in aged OA.

Overall, the absorption by organic aerosols was estimated to contribute 10-30% of the total solar absorption of

wood-combustion aerosols, where 10% represents the primary OA and 30% the aged OA. SOA formation in

biomass burning plumes is therefore an atmospherically relevant source of BrC.

646

References

648 Alexander, D. T. L., Crozier, P. A. and Anderson, J. R.: Brown carbon spheres in East Asian outflow and their
649 optical properties., Science, 321(5890), 833–6, doi:10.1126/science.1155296, 2008.

650 Andreae, M. O. and Gelencsér, A.: Black carbon or brown carbon? the nature of light-absorbing carbonaceous
651 aerosols, Atmos. Chem. Phys., 6(3), 3419–3463, doi:10.5194/acpd-6-3419-2006, 2006.

652 Barmet, P., Dommen, J., DeCarlo, P. F., Tritscher, T., Praplan, A. P., Platt, S. M., Prévôt, A. S. H., Donahue, N. M.
653 and Baltensperger, U.: OH clock determination by proton transfer reaction mass spectrometry at an environmental
654 chamber, Atmos. Meas. Tech., 5(3), 647–656, doi:10.5194/amt-5-647-2012, 2012.

655 Bertrand, A., Stefenelli, G., Bruns, E. A., Pieber, S. M., Prévôt, A. S. H., Wortham, H., Temime-roussel, B.,
656 Slowik, J. G., Haddad, I. El and Marchand, N.: Primary emissions and secondary aerosol production potential from
657 woodstoves for residential heating : influence of the stove technology and combustion efficiency, Atmos. Environ.,
658 169, doi:10.1016/j.atmosenv.2017.09.005, 2017.

659 Di Blasi, C.: Modeling chemical and physical processes of wood and biomass pyrolysis, Prog. Energy Combust.
660 Sci., 34(1), 47–90, doi:10.1016/j.pecs.2006.12.001, 2008.

661 Bond, T. C., Habib, G. and Bergstrom, R. W.: Limitations in the enhancement of visible light absorption due to
662 mixing state, J. Geophys. Res. Atmos., 111(20), 1–13, doi:10.1029/2006JD007315, 2006.

663 Bond, T. C., Doherty, S. J., Fahey, D. W., Forster, P. M., Berntsen, T., Deangelo, B. J., Flanner, M. G., Ghan, S.,
664 Kärcher, B., Koch, D., Kinne, S., Kondo, Y., Quinn, P. K., Sarofim, M. C., Schultz, M. G., Schulz, M.,
665 Venkataraman, C., Zhang, H., Zhang, S., Bellouin, N., Guttikunda, S. K., Hopke, P. K., Jacobson, M. Z., Kaiser, J.
666 W., Klimont, Z., Lohmann, U., Schwarz, J. P., Shindell, D., Storelvmo, T., Warren, S. G. and Zender, C. S.:
667 Bounding the role of black carbon in the climate system: a scientific assessment, J. Geophys. Res. Atmos., 118(11),
668 5380–5552, doi:10.1002/jgrd.50171, 2013.

669 Bruns, E. A., Krapf, M., Orasche, J., Huang, Y., Zimmermann, R., Drinovec, L., Močnik, G., El-Haddad, I., Slowik,
670 J. G., Dommen, J., Baltensperger, U. and Prévôt, A. S. H.: Characterization of primary and secondary wood
671 combustion products generated under different burner loads, Atmos. Chem. Phys., 15(5), 2825–2841,
672 doi:10.5194/acp-15-2825-2015, 2015.

673 Bruns, E. A., El Haddad, I., Slowik, J. G., Kilic, D., Klein, F., Baltensperger, U. and Prévôt, A. S. H.: Identification
674 of significant precursor gases of secondary organic aerosols from residential wood combustion., Sci. Rep., 6, 27881,
675 doi:10.1038/srep27881, 2016.

676 Bruns, E. A., Slowik, J. G., Haddad, I. El, Kilic, D., Klein, F., Dommen, J., Temime-Roussel, B., Marchand, N.,
677 Baltensperger, U. and Prévôt, A. S. H.: Characterization of gas-phase organics using proton transfer reaction time-
678 of-flight mass spectrometry : fresh and aged residential wood combustion emissions, Atmos. Chem. Phys., 705–720,
679 doi:10.5194/acp-17-705-2017, 2017.

680 Cavalli, F., Viana, M., Yttri, K. E., Genberg, J. and Putaud, J.-P.: Toward a standardised thermal-optical protocol for
681 measuring atmospheric organic and elemental carbon: the EUSAAR protocol, Atmos. Meas. Tech., 3(1), 79–89,
682 doi:doi:10.5194/amt-3-79-2010, 2010.

683 Chakrabarty, R. K., Moosmüller, H., Chen, L. W. A., Lewis, K., Arnott, W. P., Mazzoleni, C., Dubey, M. K., Wold,
684 C. E., Hao, W. M. and Kreidenweis, S. M.: Brown carbon in tar balls from smoldering biomass combustion, Atmos.
685 Chem. Phys., 10(13), 6363–6370, doi:10.5194/acp-10-6363-2010, 2010.

686 Chakrabarty, R. K., Arnold, I. J., Francisco, D. M., Hatchett, B., Hosseinpour, F., Loria, M., Pokharel, A. and
687 Woody, B. M.: Black and brown carbon fractal aggregates from combustion of two fuels widely used in asian
688 rituals, J. Quant. Spectrosc. Radiat. Transf., 122, 25–30, doi:10.1016/j.jqsrt.2012.12.011, 2013.

689   Chen, Y. and Bond, T. C.: Light absorption by organic carbon from wood combustion, Atmos. Chem. Phys., 10,
690   1773-1787, doi:10.5194/acp-10-1773-2010, 2010.

691   China, S., Mazzoleni, C., Gorkowski, K., Aiken, A. C., and Dubey, M. K.: Morphology and mixing state of
692   individual freshly emitted wildfire carbonaceous particles, Nat. Commun., 4, 1–7, doi:10.1038/ncomms-3122-2013,
693   2013.

694   Ciarelli, G., Haddad, I. El, Bruns, E. and Aksoyoglu, S., Möhler, O., Baltensperger, U. and Prévôt, A. S. H.:
695   Constraining a hybrid volatility basis set model for aging of wood burning emissions using smog chamber
696   experiments, Geosci. Model. Dev., 2303-2320, doi:10.5194/gmd-2303-2017, 2017.

697   Clarke, A., McNaughton, C., Kapustin, V., Shinozuka, Y., Howell, S., Dibb, J., Zhou, J., Anderson, B. E.,
698   Brekhovskikh, V., Turner, H. and Pinkerton, M.: Biomass burning and pollution aerosol over North America:
699   organic components and their influence on spectral optical properties and humidification response, J. Geophys. Res.
700   Atmos., 112(12), 1–13, doi:10.1029/2006JD007777, 2007.

701   Collaud Coen, M., Weingartner, E., Apituley, A., Ceburnis, D., Fierz-Schmidhauser, R., Flentje, H., Henzing, J. S.,
702   Jennings, S. G., Moerman, M., Petzold, A., Schmid, O., and Baltensperger, U.: Minimizing light absorption
703   measurement artifacts of the Aethalometer: evaluation of five correction algorithms, Atmos.Meas. Tech., 3, 457–
704   474, doi:10.5194/amt-3-457-2010, 2010.
705
706   Corbin, J. C., Lohmann, U., Sierau, B., Keller, A., Burtscher, H. and Mensah, A. A.: Black carbon surface oxidation
707   and organic composition of beech-wood soot aerosols, Atmos. Chem. Phys., 15(20), 11885–11907, doi:10.5194/acp-
708   15-11885-2015, 2015a.

709   Corbin, J. C., Keller, A., Lohmann, U., Burtscher, H., Sierau, B. and Mensah, A. A.: Organic emissions from a wood
710   stove and a pellet stove before and after simulated atmospheric aging, Aerosol Sci. Technol., 49(11), 1037–1050,
711   doi:10.1080/02786826.2015.1079586, 2015b.

712   Corbin, J. C.; Pieber, S. M.; Czech, H.; Zanatta, M.; Jakobi, G.; Massabò, D.; Orasche, J.; El Haddad, I.; Mensah, A.
713   A.; Stengel, B.; Drinovec, L.; Mocnik, G.; Zimmermann, R.; Prévôt, A. S. H. and Gysel, M.: Brown and black
714   carbon emitted by a marine engine operated on heavy fuel oil and distillate fuels: optical properties, size
715   distributions and emission factors, J. Geophys. Res. Atmos., 123, 6175-6195, doi:10.1029/2017JD027818, 2018.

716   DeCarlo, P. F., Kimmel, J. R., Trimborn, A., Northway, M. J., Jayne, J. T., Aiken, A. C., Gonin, M., Fuhrer, K.,
717   Horvath, T., Docherty, K. S., Worsnop, D. R. and Jimenez, J. L.: Field deployable, high resolution, time-of-flight
718   aerosol mass spectrometer, Anal. Chem., 78(24), 8281–8289, doi:8410.1029/2001JD001213, 2006.

719   Denier Van Der Gon, H. A. C., Bergström, R., Fountoukis, C., Johansson, C., Pandis, S. N., Simpson, D. and
720   Visschedijk, A. J. H.: Particulate emissions from residential wood combustion in Europe - revised estimates and an
721   evaluation, Atmos. Chem. Phys., 15(11), 6503–6519, doi:10.5194/acp-15-6503-2015, 2015.

722   Drinovec, L., Močnik, G., Zotter, P., Prévôt, A. S. H., Ruckstuhl, C., Coz, E., Rupakheti, M., Sciare, J., Müller, T.,
723   Wiedensohler, A. and Hansen, A. D. A.: The "dual-spot" aethalometer: an improved measurement of aerosol black
724   carbon with real-time loading compensation, Atmos. Meas. Tech., 8(5), 1965–1979, doi:10.5194/amt-8-1965-2015,
725   2015.

726   Feng, Y., Ramanathan, V. and Kotamarthi, V. R.: Brown carbon: a significant atmospheric absorber of solar
727   radiation, Atmos. Chem. Phys., 13(17), 8607–8621, doi:10.5194/acp-13-8607-2013, 2013.

728   Forrister, H., Liu, J., Scheuer, E., Dibb, J., Ziemba, L., Thornhill, L. K., Anderson, B., Diskin, G., Perring, A. E.,
729   Schwarz, J. P., Campuzan-Jost, P., Day, D. A., Palm, B. B., Jimenez, J. L., Nenes, A., Weber, R. J.: Evolution of
730   brown carbon in wildfire plumes, Gephys. Res. Lett.,42, 4623-4630, doi: 10.1002/2015GL063897, 2015.
731

732   Fu, J. S., Hsu, N. C., Gao, Y., Huang, K., Li, C., Lin, N. H. and Tsay, S. C.: Evaluating the influences of biomass
733   burning during 2006 BASE-ASIA: a regional chemical transport modeling, Atmos. Chem. Phys., 12(9), 3837–3855,
734   doi:10.5194/acp-12-3837-2012, 2012.

735 Grieshop, A. P., Logue, J. M., Donahue, N. M. and Robinson, A. L.: Laboratory investigation of photochemical
736 oxidation of organic aerosol from wood fires – part 1: measurement and simulation of organic aerosol evolution,
737 Atmos. Chem. Phys., 9, 2227–2240, doi:10.5194/acp-9-2227-2009, 2009.

738 Gueymard, C.; Myers, D.; Emery, K.: Proposed Reference Irradiance Spectra for Solar Energy Systems Testing,
739 Solar Energy, 73, 6, 443–467, 2002.
740

741 Gundel, L. A., Dod, R. L., Rosen, H. and Novakov.: The relationship between optical attenuation and black carbon
742 concentration for ambient and source particles, Sci. Total Environ., 36, 197-202, 1984.

743 Haslett, S. L.; Thomas, J. C.; Morgan, W. T.; Hadden, R.; Liu, D.; Allan, J. D.; Williams, P. I.; Keita, S.; Liousse, C.
744 and Coe, H.: Highly controlled, reproducible measurements of aerosol emissions from combustion of a common
745 African biofuel source, Atmos. Chem. Phys, 385-403, doi:10.5194/acp-18-385-2018, 2018.
746

747 Hecobian, A., Zhang, X., Zheng, M., Frank, N., Edgerton, E. S. and Weber, R. J.: Water-soluble organic aerosol
748 material and the light-absorption characteristics of aqueous extracts measured over the southeastern United States,
749 Atmos. Chem. Phys., 10(13), 5965–5977, doi:10.5194/acp-10-5965-2010, 2010.

750 Heringa, M. F., DeCarlo, P. F., Chirico, R., Tritscher, T., Dommen, J., Weingartner, E., Richter, R., Wehrle, G.,
751 Prévôt, A. S. H. and Baltensperger, U.: Investigations of primary and secondary particulate matter of different wood
752 combustion appliances with a high-resolution time-of-flight aerosol mass spectrometer, Atmos. Chem. Phys.,
753 11(12), 5945–5957, doi:10.5194/acp-11-5945-2011, 2011.

754 Hoffer, A., Gelencsér, A., Guyon, P., Kiss, G., Schmid, O., Frank, G. P., Artaxo, P. and Andreae, M. O.: Optical
755 properties of humic-like substances (HULIS) in biomass-burning aerosols, Atmos. Chem. Phys., 6, 3563-3570,
756 doi:10.5194/acp-6-3563-2006, 2006.

757 Jo, D. S., Park, R. J., Lee, S., Kim, S. W. and Zhang, X.: A global simulation of brown carbon: Implications for
758 photochemistry and direct radiative effect, Atmos. Chem. Phys., 16(5), 3413–3432, doi:10.5194/acp-16-3413-2016,
759 2016.

760 Kirchstetter, T. W., Novakov, T. and Hobbs, P. V.: Evidence that the spectral dependence of light absorption by
761 aerosols is affected by organic carbon, J. Geophys. Res. D Atmos., 109(21), 1–12, doi:10.1029/2004JD004999,
762 2004.

763 Krapf, M., Haddad, I. El, Bruns, E. A., Haddad, I. El, Molteni, U., Daellenbach, K. R., Prévôt, A. S. H.,
764 Baltensperger, U., Dommen, J. : Labile peroxides in secondary organic aerosol labile peroxides in secondary organic
765 aerosol, Chem 1, 603–616, doi:10.1016/j.chempr.2016.09.007, 2016.

766 Lack, D. A. and Langridge, J. M.: On the attribution of black and brown carbon light absorption using the Ångström
767 exponent, Atmos. Chem. Phys., 13(20), 10535–10543, doi:10.5194/acp-13-10535-2013, 2013.

768 Lambe, A. T., Cappa, C. D., Massoli, P., Onasch, T. B., Forestieri, S. D., Martin, A. T., Cummings, M. J.,
769 Croasdale, D. R., Brune, W. H., Worsnop, D. R. and Davidovits, P.: Relationship between oxidation level and
770 optical properties of secondary organic aerosol, Environ. Sci. Technol., 47(12), 6349–6357, doi:10.1021/es401043j,
771 2013.

772 Laskin, A., Laskin, J. and Nizkorodov, S. A.: Chemistry of atmospheric brown carbon, Chem. Rev., 115(10), 4335–
773 4382, doi:10.1021/cr5006167, 2015.

774 Lee, H. J., Aiona, P. K., Laskin, A., Laskin, J. and Nizkorodov, S. A.: Effect of solar radiation on the optical
775 properties and molecular composition of laboratory proxies of atmospheric brown carbon, Environ. Sci. Technol.,
776 48(17), 10217–10226, doi:10.1021/es502515r, 2014.

777 Lewis, K., Arnott, W. P., Moosmüller, H. and Wold, C. E.: Strong spectral variation of biomass smoke light
778 absorption and single scattering albedo observed with a novel dual-wavelength photoacoustic instrument, J.

779   Geophys. Res. Atmos., 113(16), 1–14, doi:10.1029/2007JD009699, 2008.

780   Lin, G., Penner, J. E., Flanner, M. G., Sillman, S., Xu, L. and Zhou, C.: Radiative forcing of organic aerosol in the
781   atmosphere and on snow: effect of SOA and brown carbon, J. Geophys. Res. - Atmos., 119(12), 7453–7476,
782   doi:10.1002/2013JD021186.Received, 2014.

783   Liu, J., Scheuer, E., Dibb, J., Ziemba, L. D., Thornhill, K. L., Anderson, B. E., Wisthaler, A., Mikoviny, T., Devi, J.
784   J., Bergin, M. and Weber, R. J.: Brown carbon in the continental troposphere, Geophys. Res. Lett., 41, 2191–2195,
785   doi:10.1002/2013GL058976, 2014.

786   Liu, J., Lin, P., Laskin, A., Laskin, J., Kathmann, S. M., Wise, M., Caylor, R., Imholt, F., Selimovic, V. and
787   Shilling, J. E.: Optical properties and aging of light absorbing secondary organic aerosol, Atmos. Chem. Phys., 16,
788   12815-12827, doi:10.5194/acp-2016-482, 2016.

789   Liu, D. T., Whitehead, J., Alfarra, M. R., Reyes-Villegas, E., Spracklen, D. V., Reddington, C. L., Kong, S. F.,
790   Williams, P. I., Ting, Y. C., Haslett, S., Taylor, J. W., Flynn, M. J., Morgan, W. T., McFiggans, G., Coe, H., and
791   Allan, J. D.: Black-carbon absorption enhancement in the atmosphere determined by particle mixing state, Nat.
792   Geosci., 10, 184–188, doi:10.1038/ngeo2901, 2017.
793

794   Liu, P. F., Abdelmalki, N., Hung, H. M., Wang, Y., Brune, W. H. and Martin, S. T.: Ultraviolet and visible complex
795   refractive indices of secondary organic material produced by photooxidation of the aromatic compounds toluene and
796   m-xylene, Atmos. Chem. Phys., 15(3), 1435–1446, doi:10.5194/acp-15-1435-2015, 2015a.

797   Liu, P. S. K., Deng, R., Smith, K. A., Jayne, J. T., Williams, L.R., Canagaratna, M. R., Moore, K., Onasch, T. B.,
798   Worsnop, D.R., and Deshler, T.: Transmission efficiency of an aerodynamic focusing lens system: comparison of
799   model calculations and laboratory measurements for the aerodyne aerosol mass spectrometer,Aerosol Sci. Tech., 41,
800   721–733, 2007.
801

802   Liu, S., Aiken, A. C., Gorkowski, K., Dubey, M. K., Cappa, C. D., Williams, L. R., Herndon, S. C., Massoli, P.,
803   Fortner, E. C., Chhabra, P. S., Brooks, W. A., Onasch, T. B., Jayne, J. T., Worsnop, D. R., China, S., Sharma, N.,
804   Mazzoleni, C., Xu, L., Ng, N. L., Liu, D., Allan, J. D., Lee, J. D., Fleming, Z. L., Mohr, C., Zotter, P., Szidat, S. and
805   Prévôt, A. S. H.: Enhanced light absorption by mixed source black and brown carbon particles in UK winter, Nat.
806   Commun., 8435, doi:10.1038/ncomms9435, 2015b.

807   Lu, Z., Streets, D. G., Winijkul, E., Yan, F., Chen, Y., Bond, T. C., Feng, Y., Dubey, M. K., Liu, S., Pinto, J. P. and
808   Carmichael, G. R.: Light absorption properties and radiative effects of primary organic aerosol emissions, Environ.
809   Sci. Technol., 49, 4868–4877, doi:10.1021/acs.est.5b00211, 2015.

810   Massabò, D., Caponi, L., Bernardoni, V., Bove, M. C., Brotto, P., Calzolai, G., Cassola, F., Chiari, M., Fedi, M. E.,
811   Fermo, P., Giannoni, M., Lucarelli, F., Nava, S., Piazzalunga, A., Valli, G., Vecchi, R. and Prati, P.: Multi-
812   wavelength optical determination of black and brown carbon in atmospheric aerosols, Atmos. Environ., 108, 1–12,
813   doi:10.1016/j.atmosenv.2015.02.058, 2015.

814   Massabò, D., Bernardoni, V., Bove, M. C., Brunengo, A., Cuccia, E., Piazzalunga, A., Prati, P., Valli, G. and
815   Vecchi, R.: A multi-wavelength optical set-up for the characterization of carbonaceous particulate matter, J. Aerosol
816   Sci., 60, 34–46, doi:10.1016/j.jaerosci.2013.02.006, 2013.

817   Moosmüller, H., Chakrabarty, R. K. and Arnott, W. P.: Aerosol light absorption and its measurement: A review, J.
818   Quant. Spectrosc. Radiat. Transf., 110(11), 844–878, doi:10.1016/j.jqsrt.2009.02.035, 2009.

819   Moosmüller, H., Chakrabarty, R. K., Ehlers, K. M. and Arnott, W. P.: Absorption Ångström coefficient, brown
820   carbon, and aerosols: Basic concepts, bulk matter, and spherical particles, Atmos. Chem. Phys., 11(3), 1217–1225,
821   doi:10.5194/acp-11-1217-2011, 2011.

822   Petzold, A. and Schönlinner, M.: Multi-angle absorption photometry - A new method for the measurement of
823   aerosol   light   absorption   and   atmospheric   black   carbon,   J.   Aerosol   Sci.,   35(4),   421–441,

824   doi:10.1016/j.jaerosci.2003.09.005, 2004.

825   Platt, S. M., El Haddad, I., Zardini, A. A., Clairotte, M., Astorga, C., Wolf, R., Slowik, J. G., Temime-Roussel, B.,
826   Marchand, N., Ježek, I., Drinovec, L., Močnik, G., Möhler, O., Richter, R., Barmet, P., Bianchi, F., Baltensperger,
827   U. and Prévôt, A. S. H.: Secondary organic aerosol formation from gasoline vehicle emissions in a new mobile
828   environmental reaction chamber, Atmos. Chem. Phys., 13(18), 9141–9158, doi:10.5194/acp-13-9141-2013, 2013.

829   Romonosky, D. E., Laskin, A., Laskin, J. and Nizkorodov, S. A.: High-resolution mass spectrometry and molecular
830   characterization of aqueous photochemistry products of common types of secondary organic aerosols, J. Phys.
831   Chem. A, 119(11), 2594–2606, doi:10.1021/jp509476r, 2015.

832   Saleh, R., Hennigan, C. J., McMeeking, G. R., Chuang, W. K., Robinson, E. S., Coe, H., Donahue, N. M. and
833   Robinson, A. L.: Absorptivity of brown carbon in fresh and photo-chemically aged biomass-burning emissions,
834   Atmos. Chem. Phys., 13(15), 7683–7693, doi:10.5194/acp-13-7683-2013, 2013.

835   Saleh, R., Robinson, E. S., Tkacik, D. S., Ahern, A. T., Liu,S., Aiken, A. C., Sullivan, R. C., Presto, A. A., Dubey,
836   M. K., Yokelson, R. J., Donahue, N. M., and Robinson, A.L.: Brownness of organics in aerosols from biomass
837   burning linked to their black carbon content, Nat. Geosci., 7, 2–5, doi:10.1038/ngeo2220, 2014.
838

839   Schauer, J. J., Mader, B. T., Deminter, J. T., Heidemann, G., Bae, M. S., Seinfeld, J. H., Flagan, R. C., Cary, R. A.,
840   Smith, D., Huebert, B. J., Bertram, T., Howell, S., Kline, J. T., Quinn, P., Bates, T., Turpin, B., Lim, H. J., Yu, J. Z.,
841   Yang, H., and Keywood, M. D.: ACE-Asia intercomparison of a thermaloptical method for the determination of
842   particle-phase organic and elemental carbon, Environ. Sci. Technol., 37, 993–1001, 2003.
843

844   Shafizadeh, F.: The chemistry of pyrolysis and combustion. The chemistry of solid Wood, ACS Symp. Ser., 207,
845   489–529, doi:10.1021/ba-1984-0207.ch013\r10.1021/ba-1984-0207.ch013, 1984.

846   Slowik, J. G., E. S. Cross, J.-H. Han, P. Davidovits, T. B. Onasch, J. T. Jayne, L. R. Williams, M. R. Canagaratna,
847   D. R. Worsnop, R. K. Chakrabarty, H. Moosmüller, W. P. Arnott, J. P. Schwarz, R. S. Gao, D. W. Fahey, G. L. Kok
848   and A. Petzold.: An inter-comparison of instruments measuring black carbon content of soot particles, *Aerosol Sci.*
849   *Technol. 41*, 3, 295-314, 2007.
850

851   Sumlin, B. J., Pandey, A., Walker, M. J., Pattison, R. S., Williams, B. J., and Chakrabarty, R. K.: Atmospheric
852   photooxidation diminishes light absorption by primary brown carbon aerosol from biomass burning, Environ. Sci.
853   Technol. Lett., 4(12), 540-545, doi:10.1021/acs.estlett.7b00393, 2017.

854   Sun, H., Biedermann, L. and Bond, T. C.: Color of brown carbon: A model for ultraviolet and visible light
855   absorption by organic carbon aerosol, Geophys. Res. Lett., 34(17), 1–5, doi:10.1029/2007GL029797, 2007.

856   Ulevicius, V., Bozzetti, C., Vlachou, A., Plauškait, K., Mordas, G., Dudoitis, V., Abbaszade, G., Remeikis, V.,
857   Garbaras, A., Masalaite, A., Blees, J., Fröhlich, R., Dällenbach, K. R., Canonaco, F., Slowik, J. G., Dommen, J.,
858   Zimmermann, R., Schnelle-kreis, J., Salazar, G. A. and Agrios, K., Szidat, S., Haddad, I. El., and Prévôt, A. S. H. :
859   Fossil and non-fossil source contributions to atmospheric carbonaceous aerosols during extreme spring grassland
860   fires in Eastern Europe, Atmos. Chem. Phys., 16, 5513–5529, doi:10.5194/acp-16-5513-2016, 2016.

861   Wang, X., Heald, C. L., Ridley, D. A., Schwarz, J. P., Spackman, J. R., Perring, A. E., Coe, H., Liu, D. and Clarke,
862   A. D.: Exploiting simultaneous observational constraints on mass and absorption to estimate the global direct
863   radiative forcing of black carbon and brown carbon, Atmos. Chem. Phys., 14(20), 10989–11010, doi:10.5194/acp-
864   14-10989-2014, 2014.

865   Weingartner, E., Saathoff, H., Schnaiter, M., Streit, N., Bitnar, B. and Baltensperger, U.: Absorption of light by soot
866   particles: determination of the absorption coefficient by means of aethalometers, J. Aerosol Sci., 34(10), 1445–1463,
867   doi:10.1016/S0021-8502(03)00359-8, 2003.

868   Yang, H. and Yu, J. Z.: Uncertainties in charring correction in the analysis of elemental and organic carbon in
869   atmospheric particles by thermal/optical methods, Environ. Sci. Technol., 36 (23), 5199–5204, 2002.
870

871 Zhang, X., Lin, Y. –H., Surratt, J. D., Zotter, P. and Prévôt, A. S. H.: Light-absorbing soluble organic aerosol in
872 Los-Angeles and Atlanta: A contrast in secondary organic aerosol, Geophys. Res. Lett, 38, 2011.
873
874 Zhao, R., Lee, A. K. Y., Huang, L., Li, X., Yang, F. and Abbatt, J. P. D.: Photochemical processing of aqueous
875 atmospheric brown carbon, Atmos. Chem. Phys., 15(11), 6087–6100, doi:10.5194/acp-15-6087-2015, 2015.

876 Zotter, P., Herich, H., Gysel, M., El-Haddad, I., Zhang, Y., Močnik, G., Hüglin, C., Baltensperger, U., Szidat, S. and
877 Prévôt, A. S. H.: Evaluation of the absorption Ångström exponents for traffic and wood burning in the Aethalometer
878 based source apportionment using radiocarbon measurements of ambient aerosol, Atmos. Chem. Phys., 17, 4229-
879 4249, doi:10.5194/acp-17-4229-2017, 2017.

880 Zotter, P., Herich, H., Gysel, M., El-haddad, I., Zhang, Y. and Močnik, G.: Evaluation of the absorption Ångström
881 exponents for traffic and wood burning in the Aethalometer-based source apportionment using radiocarbon
882 measurements of ambient aerosol, , 4229–4249, doi:10.5194/acp-17-4229-2017, 2017.

883
884

885

886

887

888

889

890

891

892

893

894

895

896

897

898

899

900

901

902

903

904

905

906

907
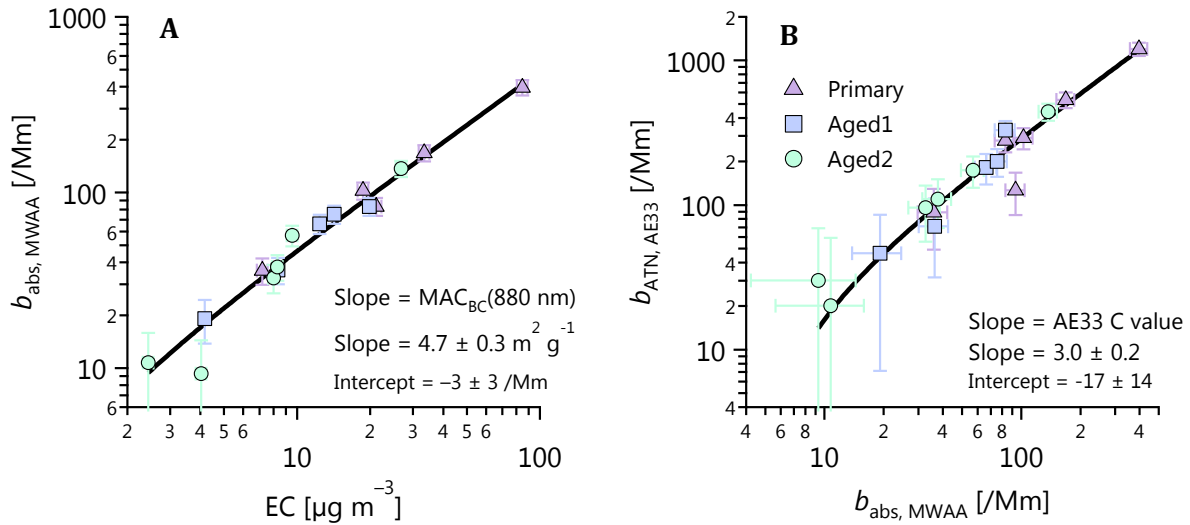
Figure 1: Determination of (A) MAC_{BC}(880nm) and (B) aethalometer C value using MWAA absorption measurements, thermal/optical EC (EUSAAR2 protocol) and aethalometer attenuation measurements. MWAA absorption measurements at 880 nm is determined by extrapolating the absorption coefficients at 850 nm using an α determined from the ratio between the absorption coefficients at 850 nm and 635nm. The aerosols were either primary (no OH exposure), Aged 1 ($\sim 1 \times 10^7$ molec OH cm^{-3} h), or Aged 2 ($\sim 4 \times 10^7$ molec OH cm^{-3} h). No difference in MAC or C value was discernable with aging (see also Fig. S2). The C value derived from σ_{ATN} recommended by Drinovec et al. (2015) = 2.6 compares well with the value derived in Fig. 1B.

915

916

917

918

919

920

921
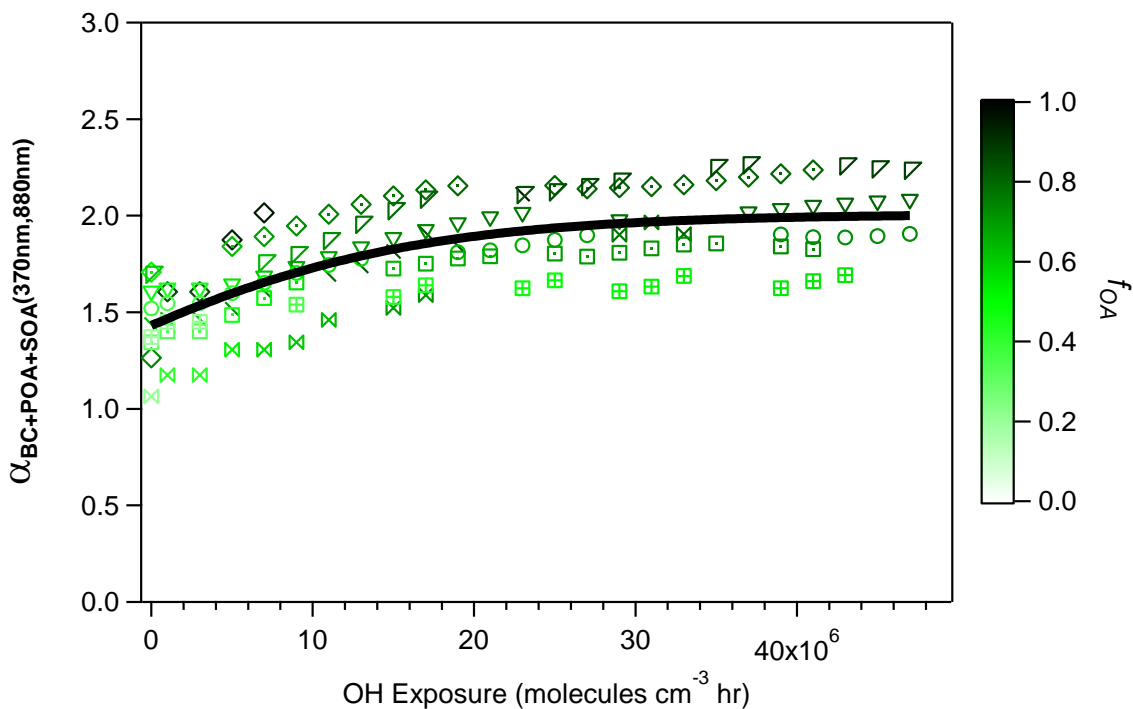
Figure 2: Evolution during photochemical aging of $\alpha_{BC+POA+SOA}(370nm, 880nm)$ (two-wavelength Ångström exponent calculated using total absorption data at 370 nm and 880 nm), where the different symbols denote individual experiments. Data are colored by the OA mass fraction $f_{OA} = M_{OA}/(M_{OA} + M_{BC})$. The black line is a fit to guide the eye.

925

926
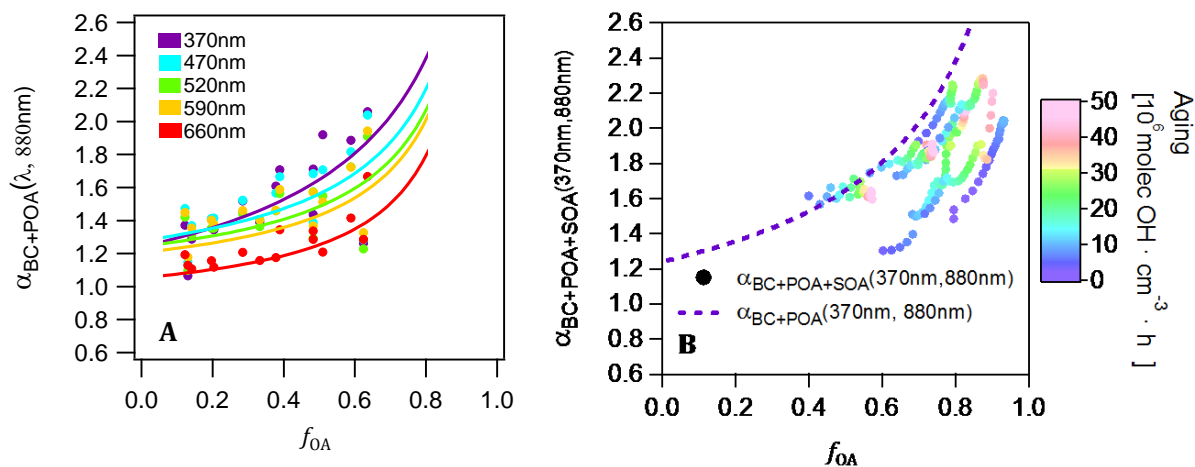
Figure 3: (A) Relationship of α_{BC+POA} (λ, 880nm) to f_{OA} for seven wavelengths for primary emissions. Data are colored by the wavelength. Curves are fits of Eq. (13) to the data. Each point represents the average of one experiment and therefore the variability in f_{OA} is related to the variability in the emission composition between experiments. (B) Relationship of $\alpha_{BC+POA+SOA}(370nm, 880nm)$ to f_{OA} for several experiments for aged aerosols. Data are color coded by the OH exposure. The variability in f_{OA} is due to SOA formation with aging; data from several experiments are shown which explains the wide range of f_{OA} at low OH exposures. Note that more data are included in A than B, as primary emissions for some experiments were not aged.

934

935

33

936
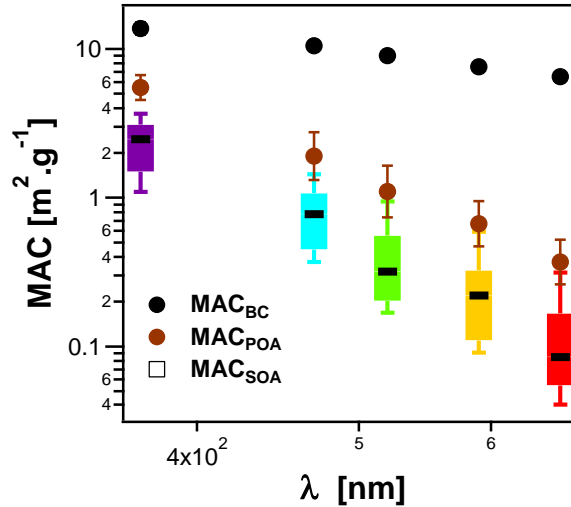
Figure 4: MAC$_{SOA}$(λ) calculated from several smog chamber experiments plotted as box-whiskers as a function of wavelength (also shown by the color of the bars). The thick black lines, the boxes and the whiskers mark the medians, the quartiles and the 10th and the 90th percentiles, respectively. Also shown are the MAC$_{BC}$(λ) and MAC$_{POA}$(λ) reported in Table 1. Note that MAC$_{SOA}$(880nm) and MAC$_{POA}$(880nm) are zero by definition.

941

942
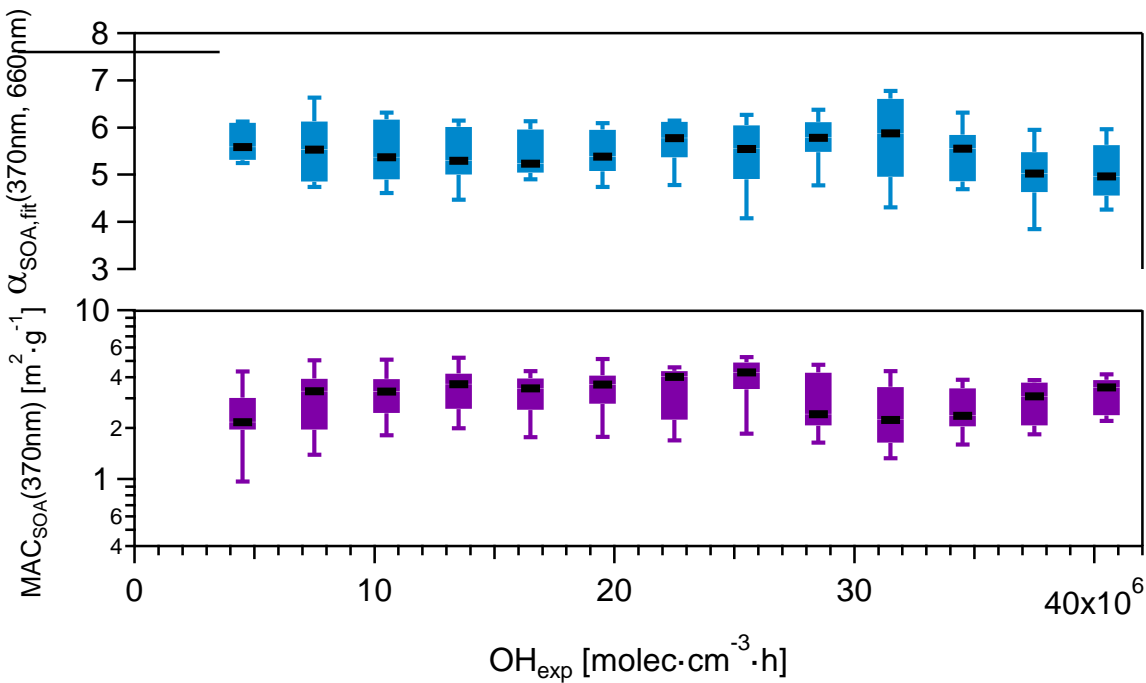
Figure 5: MAC$_{SOA}$(370nm) and $\alpha_{SOA,fit}$(370nm, 660nm) calculated from several smog chamber experiments plotted as a function of OH exposure. The box marks the 25th and 75th percentile, while the whiskers mark the 10th and the 90th percentile. MAC$_{SOA}$(370nm) was obtained using Eq. (19). $\alpha_{SOA,fit}$(370nm, 660nm) was obtained from fitting the MAC$_{SOA}$ values in the range 370-660 nm for the different experiments against the wavelength. $\alpha_{SOA,fit}$(370nm, 660nm) is the slope of the linear fit applied after log transforming the data. MAC$_{SOA}$(λ) for higher wavelengths are shown in Fig. S10.

948

949

950

34

951

952
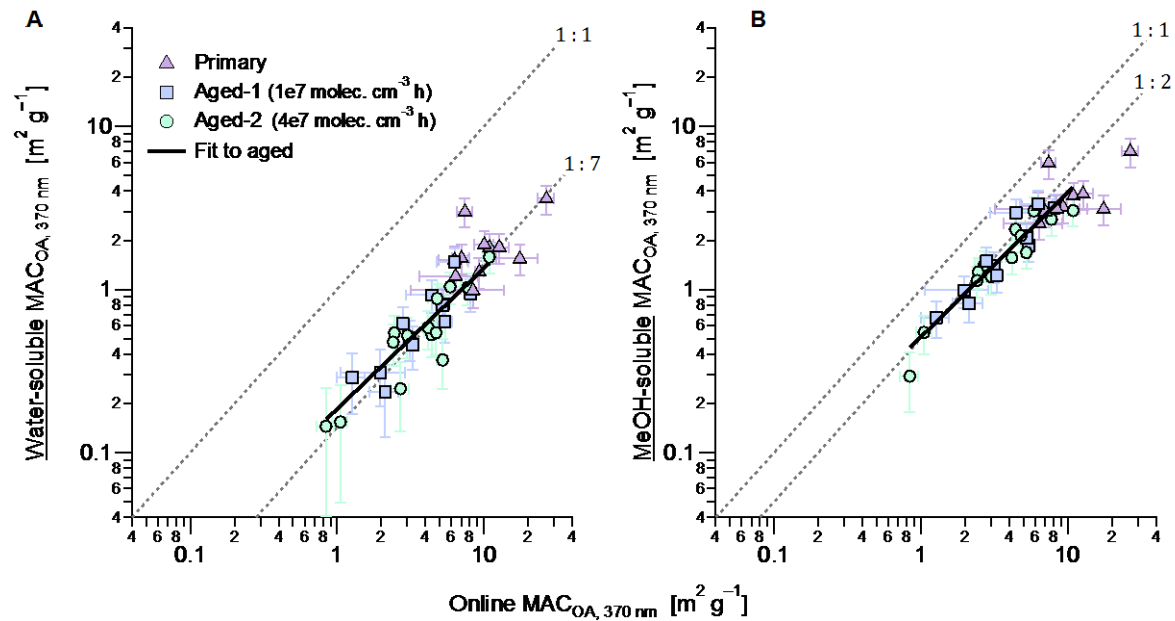
Figure 6: Comparison of the MAC_{OA}(370nm) of aged aerosols determined from online and offline absorption measurements. The offline filter-extraction method directly quantified properties of total OA (ordinate), while the average of MAC_{SOA} and MAC_{POA} weighted with respective mass concentrations is shown on the abscissa. The panels show offline measurements of (A) water-soluble OA, (B) methanol-soluble OA. Fits are to aged data only due to the significantly smaller scatter of those data, although primary data on average follow similar trends. The fitted slopes and intercepts are, respectively, (A) 0.13 ± 0.02 and 0.05 ± 0.06 m^2g^{-1} and (B) 0.12 ± 0.1 and 0.38 ± 0.03 m^2g^{-1}.

959

960

961
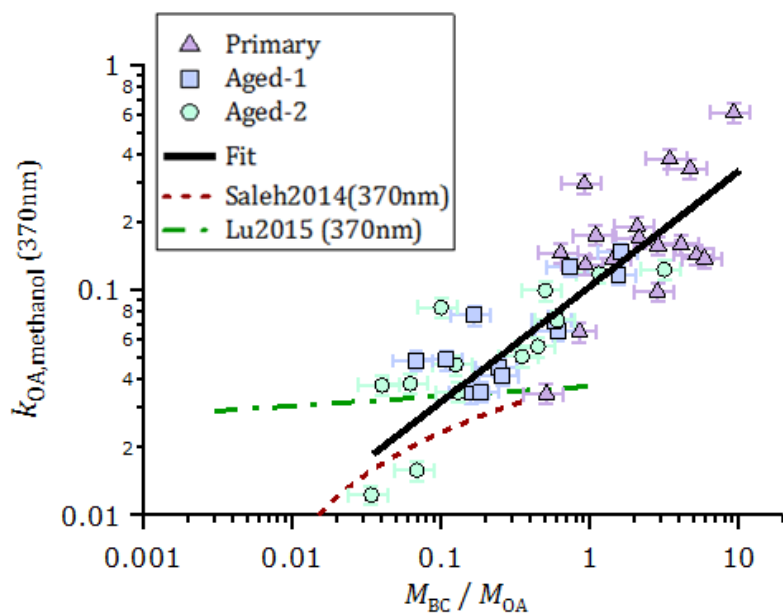
Figure 7: Imaginary part of the OA refractive index at 370 nm, obtained from offline UV/vis spectroscopy of methanol OA extracts, plotted as a function of f_{OA}. The data could be empirically represented by a linear function in the log-log space, in the measurement range. The ordinary least-squares fit is $(k_{OA,nm}) = \log(M_{BC}/M_{OA})(0.51\pm0.07) + (-0.98\pm0.05)$. Also shown are parameterizations of $k_{OA}(370$ nm) for open burning against M_{BC}/M_{OA} estimated based on the online k_{OA} (550 nm) measurements in Saleh et al. (2014) and Lu et al. (2015), using the k_{OA} wavelength dependence reported by the respective authors.

968

969

970
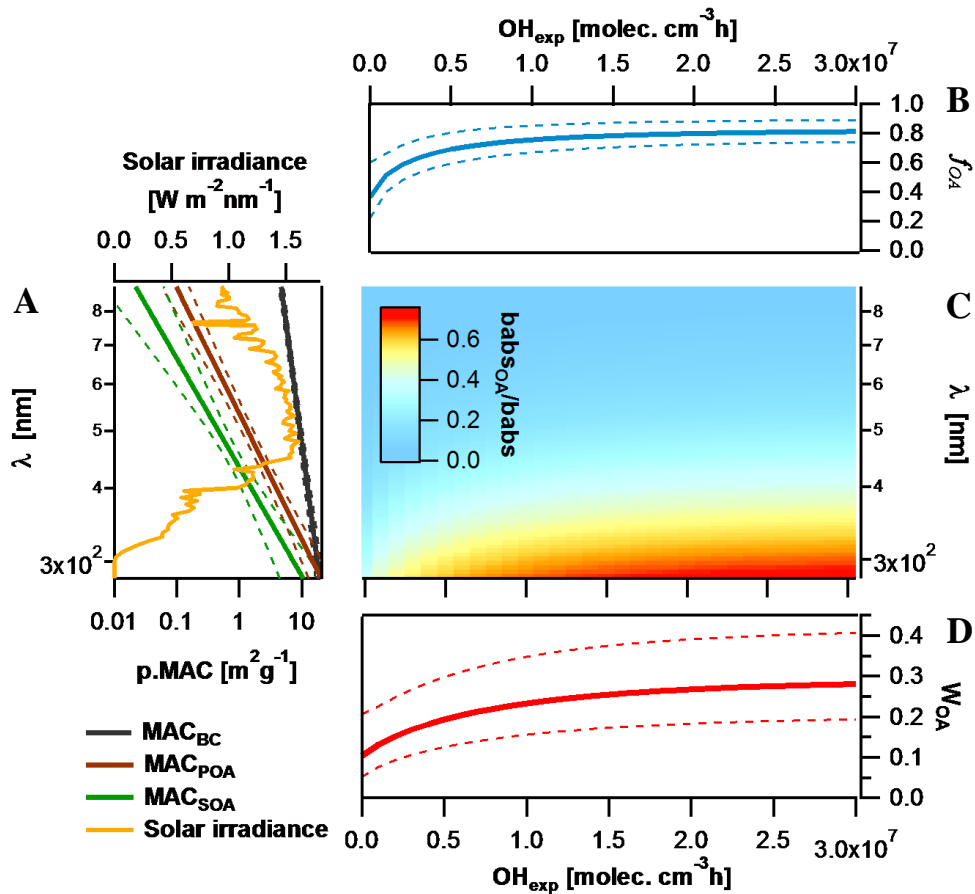
Figure 8: Impact of BrC absorption on total primary and secondary wood-burning-aerosol absorption. (A) MACs of different particle components (BC, POA and SOA) along with their corresponding standard deviations plotted as a function of wavelength based on smog chamber data and compared to the solar irradiance spectrum. **(B)** Species average relative abundance in the smog chamber (f_{OA}) plotted as a function of the OH exposure. **(C)** Image plot showing the OA absorption coefficient relative to the total aerosol absorption as a function of wavelength and OH exposure. **(D)** Rate of energy transfer due to BrC light absorption relative to the total carbonaceous aerosol absorption (W_{OA}) estimated as a function of aging using the solar flux, the fractions of the different components and their MACs.

990

Table 1: Geometric mean and standard deviations of the determined MACs of BC, POA and SOA at different wavelengths. Uncertainties were obtained from fits of Eq. (13) for MAC_{BC}, MAC_{POA}, while for MAC_{SOA} uncertainties GSD values are geometric standard deviation values on the MAC_{SOA} average values from all experiments. These uncertainties do not include uncertainties related to the determination of MAC_{BC}(880nm). By definition, BrC absorbance at 880 nm is zero.

	BC		POA		SOA	
λ (nm)	GM (m^2 g^{-1})	GSD	GM (m^2 g^{-1})	GSD	GM (m^2 g^{-1})	GSD
370	13.7	1.1	5.5	1.21	2.2	1.39
470	10.5	1.06	1.9	1.45	0.72	1.61
520	9	1.04	1.1	1.49	0.34	1.75
590	7.6	1.03	0.67	1.42	0.2	1.97
660	6.5	1.01	0.37	1.41	0.09	2.42
880	4.6	0.7	0*		0*	

*By definition

997